5

Mars tectonics

Matthew P. Golombek
Jet Propulsion Laboratory, California Institute of Technology, Pasadena

and

Roger J. Phillips
Planetary Science Directorate, Southwest Research Institute, Boulder

Summary

Mars is a key intermediate-sized terrestrial planet that has maintained tectonic (and overall geologic) activity throughout its history, and preserved a record in rocks and terrains exposed at the surface. Among the earliest recorded major geologic events was lowering of the northern plains, relative to the southern highlands, possibly by a giant, oblique impact (or endogenic process) that left an elliptical basin with a thinned crust. Sitting on the edge of this global crustal dichotomy is Tharsis, an enormous elevated volcanic and tectonic bulge that rises ~10 km above the datum. It is topped by four giant shield volcanoes, and is surrounded by radial extensional grabens and rifts and concentric compressional wrinkle ridges that together deform the entire western hemisphere and northern plains. Deformation in the eastern hemisphere is more localized in and around large impact basins and volcanic provinces. Extensional structures are dominantly narrow grabens (several kilometers wide) that individually record of order 100 m extension, although larger (100 km wide), deeper rifts are also present. Compressional structures are dominated by wrinkle ridges, interpreted to be folds overlying blind thrust faults that individually record shortening of order 100 m, although larger compressional ridges and lobate scarps (thrust fault scarps) have also been identified. Strike-slip faults are relatively rare and typically form in association with wrinkle ridges or grabens. Mapping of extensional structures in deformed regions that have rich stratigraphies shows that structures on Mars formed during five main stages: (1) Noachian deformation concentrated in Claritis Fossae, Thaumasia, Sirenum, Syria Planum, Ceraunius, and Tempe Terra; (2) Late Noachian – Early Hesperian deformation concentrated

Planetary Tectonics, edited by Thomas R. Watters and Richard A. Schultz. Published by Cambridge University Press.

in Valles Marineris and Thaumasia; (3) Early Hesperian deformation concentrated in Noctis Labyrinthus, Tempe Terra, Valles Marineris, and Thaumasia; (4) Late Hesperian – Early Amazonian deformation concentrated in Alba Patera, Tempe Terra, and around Olympus Mons and the Tharsis Montes; and (5) Middle–Late Amazonian deformation concentrated around the large shield volcanoes. About half of the extensional structures formed during the Noachian (>3.8 Ga), indicating that tectonic activity peaked early and generally decreased with time. Wrinkle-ridge formation peaked in the Hesperian (both around Tharsis and in the eastern hemisphere, far from Tharsis), suggesting an overprint and modulation by global compressional cooling stresses. Lithospheric deformation models resulting from elastic-shell loading show that loading over the scale of Tharsis (large relative to the radius of the planet) is dominated by membrane stresses, and produces the concentric extensional stresses around the periphery and the radial compressional stresses closer in that are needed to explain the radial grabens and rifts and concentric wrinkle ridges. Because elastic-shell models based on present-day gravity and topography can explain the observed distribution and strain of radial (over half of which are Noachian) and concentric tectonic features, the basic lithospheric structure of the province has probably changed little since the Noachian and elastic support of the Tharsis load by a thickening lithosphere has been the dominant geodynamical mechanism. The origin of Tharsis required a positively buoyant mantle region accompanied by voluminous partial melting, of which a core–mantle plume is one possibility. This enormous volcanic load produced a moat around it, which shows up most dramatically as a negative gravity ring, and an antipodal bulge that contributes to the first-order shape and gravity field of the planet. If the load is composed of basaltic magmatic products as suggested by fine layers within Valles Marineris, water released with the magma would be equivalent to a global layer up to 100 m thick, which might have enabled the early warm and wet Martian climate indicated by valley networks, degraded craters and terrains, sulfates, and phyllosilicates found by rovers and orbiters exploring Mars. Additional geophysical constraints on Tharsis include the observation that remanent magnetic anomalies occur high on the Tharsis rise and likely require uplift of the Tharsis crust early in its evolution.

1 Introduction

Because of its intermediate size, Mars is a key planet among our solar system's collection of terrestrial planets. It is large enough to have had geologic and tectonic activity throughout geologic time, but not so active as to have totally destroyed all record of its early geologic history. Because most geologic and tectonic processes are driven by the internal heat engine of a planet or satellite, large planets such as the Earth and Venus have had active and prolonged geological histories due

to their greater volume to surface area ratio (proportional to radiogenic heat flux) than the small planetary bodies such as the Moon and Mercury (Kaula, 1975). Of our assortment of terrestrial planets, the Earth and Venus have been so active that most of their early histories have been destroyed by ongoing vigorous geologic activity. In contrast, Mercury and the Moon have largely cratered surfaces with little geologic activity after the first ∼2 Ga. Mars appears to be just the right size to have maintained geologic and tectonic activity throughout time, and to have preserved the record in rocks and terrains exposed at the surface for study.

On Earth, it is now accepted that the plate tectonic system has directly modulated and maintained clement conditions and liquid oceans for most of geologic time and thus has been important for the evolution of life (Ward and Brownlee, 2000, 2002). Plate tectonics has maintained a constant freeboard or relative level of exposed continents and oceans throughout the Phanerozoic (Wise, 1974) by liberating, through subduction, volatiles trapped in weathered rocks, and has controlled the level of greenhouse gases in the atmosphere. Without this process, volatiles can be trapped in weathering products and lost from the atmosphere and hydrosphere, resulting in a dry, waterless climate.

On Mars, it is therefore perhaps not surprising that there is growing evidence that its tectonic evolution has been critically important to its climatic history (Phillips *et al*., 2001). During the early history of Mars (Plate 14) – the oldest geologic period is the Noachian, estimated by crater density to be >3.6 Ga (Hartmann and Neukum, 2001; Hartmann, 2005; Tanaka and Hartmann, 2008) – there is abundant evidence for wetter and possibly warmer conditions in valley networks, dry lake beds, and high erosion rates preserved in degraded craters and terrain (Carr, 1996; Craddock and Howard, 2002; Howard *et al*., 2005; Irwin *et al*., 2005). Further, surface exploration by the Mars Exploration Rovers (MER) has found sulfates in Meridiani Planum that have been interpreted as "dirty" evaporites (Squyres *et al*., 2004) (likely fed by groundwater (Andrews-Hanna *et al*., 2007)), and the aqueous alteration of rocks in the Columbia Hills (Squyres *et al*., 2006) that also indicate wetter conditions in the Late Noachian. The imaging spectrometers OMEGA on Mars Express and CRISM on the Mars Reconnaissance Orbiter have revealed the widespread occurrence of phyllosilicates in Noachian terrain (Bibring *et al*., 2006; Mustard *et al*., 2008), with clear evidence in places that this material has been excavated from the crust by impacts (Mustard *et al*., 2008). Clearly water was a pervasive commodity during the Noachian period on Mars. In contrast, the current climate is dry and desiccating, with extremely low erosion rates consistent with eolian activity, and little or no erosion by liquid water in the Hesperian (the intermediate geologic period on Mars, estimated to be 2.6–3.6 Ga) and Amazonian – the youngest geologic period, estimated to be <2.6 Ga (Hartmann and Neukum, 2001; Hartmann, 2005; Tanaka and Hartmann, 2008) (Arvidson *et al*., 1979; Golombek and Bridges, 2000; Golombek *et al*., 2006a,b; Grant *et al*., 2004) (Plate 14).

Evidence for early warmer and wetter conditions have generally fueled speculation that the early environment on Mars may have been conducive to the formation of life at a time when life started on Earth. If Mars was indeed wetter early in its history, what caused this brief more clement period and what led to its change to the current cold and dry conditions that appear to have been in place since the Hesperian? The answer to this question may be locked in the development and rise of the Tharsis province on Mars, the largest and longest lived tectonic entity in the solar system.

Any discussion of Mars tectonics centers on Tharsis and the highland–lowland dichotomy (aka global dichotomy). Tharsis is an enormous elevated region of the planet, covered by huge volcanoes and surrounded by a system of generally radial extensional tectonic features (including the huge Valles Marineris), and generally concentric compressional tectonic features that imprint the entire western hemisphere of the planet (Banerdt *et al*., 1992) and most of the northern plains (Withers and Neumann, 2001; Head *et al*., 2002). The elevated region of Tharsis covers one quarter of the planet ($\sim 3.0 \times 10^7$ km^2 in areal extent) and rises to 10 km above the Mars Orbiter Laser Altimeter (MOLA) defined geoid near Syria Planum, with young (Amazonian) shield volcanoes rising to over 20 km elevation (Smith *et al*., 2001). Tharsis appears to sit on the highland–lowland boundary that separates the northern plains that are less cratered, and therefore have a younger surface age, and are several kilometers lower than the southern highlands that are more heavily cratered and higher in elevation. Located at the edges of Tharsis and the highland–lowland boundary are the catastrophic outflow channels that funneled huge volumes of water into the northern plains, intermediate in Mars history (Hesperian and Early Amazonian) (Baker *et al*., 1992). To first order then, some process or processes lowered and resurfaced about a third of the planet to create the northern plains early in its history and another (or perhaps related) process created a huge topographic rise, topped by young volcanics that produced tectonic features that deform, to various degrees, most of the planet. The resultant major questions in Mars tectonics involve understanding the timing and causes of these two primary tectonic events.

Our understanding of the tectonics of Mars has been fueled by data returned from spacecraft that have visited the Red Planet, and is experiencing a renaissance with the data returned from the Mars Global Surveyor (MGS), Mars Odyssey, Mars Express, and Mars Reconnaissance Orbiter (MRO) spacecraft. Prior to the data returned by these spacecraft, our interpretations of structural features and tectonics have been based on Viking topography and gravity, and global imaging at $\sim$200 m/pixel scale. The imaging data allowed the mapping of regions and areas that defined the timing of structural events within the established stratigraphic framework of Mars (Tanaka, 1986). However, the poor topography and accurate

knowledge of only the lower degree gravity and topographic fields severely inhibited the realistic modeling of local and regional deformational processes. MGS has returned exquisite global topographic data from MOLA (Smith *et al*., 1999b; Smith *et al*., 2001) and gravity data accurate to spherical harmonic degree and order 60 (Smith *et al*., 1999a; Lemoine *et al*., 2001; Yuan *et al*., 2001), which have ushered in a renewed era of much more constrained modeling of deformational processes. The addition of tracking data from MRO has yielded significant improvements in the spherical harmonic gravity field and derived crustal thickness models (Zuber *et al*., 2007; Neumann *et al*., 2008). Similar advances in geologic and tectonic mapping and characterization have been realized from the high-resolution Mars Orbiter Camera (MOC on MGS), High Resolution Imaging Science Experiment (HiRISE on MRO), High Resolution Stereo Camera (HRSC on Mars Express), and Thermal Emission Imaging System (THEMIS on Odyssey) images (Golombek, 2003).

In this chapter on Mars tectonics (and associated geophysics), we begin with a description of the global geology, topography and gravity of Mars as a basis for understanding the tectonic framework of the planet. We then discuss the geometry and kinematics of structural features on Mars (extensional, compressional and strike-slip). The tectonic history of these features, including their distribution in structural terrains, timing and orientation, are next discussed for the western and eastern hemispheres of Mars. These sections then provide the basic framework to discuss deformational mechanisms at a global, regional and local scale. We will refer to, but not repeat, information in the last major review of Mars tectonics, a summary of knowledge based on the Viking data (Banerdt *et al*., 1992), and will focus on new information and advances since that publication.

2 Global geology, topography and gravity

2.1 Physiography

To first order, the major physiographic units of Mars are also distinguishable in its geology, topography and gravity (Plates 13 and 15). The three major units: the southern highlands, northern plains, and the Tharsis plateau have been known since Mariner 9 acquired imaging data in the early 1970s. The southern highlands are elevated, heavily cratered terrain that includes large impact basins (Argyre and Hellas) that date back to the end of heavy bombardment. High crater densities and mapping results place the southern highlands as ancient Noachian units most affected by the high cratering rates early in solar system history. The northern plains, separated from the highlands by the global dichotomy boundary and the Tharsis rise, are several kilometers lower in elevation and have much lower crater

densities, suggesting Late Hesperian and Amazonian surface ages that are much younger than the southern highlands (Tanaka *et al*., 2003, 2005). The physiographic boundary, where not obscured by the Tharsis rise, is in places a smooth transition from cratered terrain to volcanic/sedimentary plains, but in other places is more abrupt, showing the effects of both tectonic and erosional processes (McGill and Dimitriou, 1990; Smith *et al*., 1999b; Smrekar *et al*., 2004).

Remnants of large craters are evident in the northern plains (e.g., Isidis and Utopia) and careful inspection of MOLA topography revealed a large number of subtle circular depressions (termed "quasi-circular depressions," QCDs) that have been reasonably interpreted as shallowly buried impact craters and basins (Frey *et al*., 2002; Frey, 2006a,b). The size–frequency distributions of these circular depressions argue strongly that the underlying surface dates from before the earliest Noachian (i.e., pre-Noachian) (Nimmo and Tanaka, 2005; Frey, 2006a,b) and that the total fill in the northern plans is mostly thin (a few kilometers), suggesting that the northern plains have been low throughout virtually all of Martian history recorded in surface or near-surface terrains.

The enormous plateau of the Tharsis rise is ringed by ridged plains, interpreted as deformed Hesperian flood basalts, and capped by Amazonian lavas and shield volcanoes. The five largest volcanoes are the three central Tharsis Montes (from south to north: Arsia, Pavonis and Ascreaeus), the tallest, Olympus Mons to the northwest, and Alba Patera to the north. To the east, south and southwest of Tharsis are Noachian cratered highlands and within the plateau are portions of highlands crust surrounded by younger Amazonian volcanics (Plescia and Saunders, 1982; Scott and Tanaka, 1986). To the northeast, north and northwest of Tharsis are the lower and younger northern plains covered by Hesperian through Amazonian lava flows, sediments and outflow channel deposits. The highest portion of Tharsis, aside from the five giant volcanoes, is Syria Planum, which is bounded on the west by Claritas Fossae, a high-standing ridge of heavily fractured Noachian terrain that extends south to the Thaumasia region, and to the north by Noctis Labyrinthus, a huge system of intersecting troughs. From the eastern end of Noctis Labyrinthus open the giant canyons of Valles Marineris that cleave the Hesperian plains for 2000 km to the east before opening into a series of chaos-filled depressions. Some of the Hesperian giant catastrophic outflow channels that begin in the Noachian highlands and drain into the northern plains appear to originate in these chaos-filled depressions.

The eastern hemisphere of Mars is dominated by heavily cratered terrain to the south, and across the dichotomy boundary lie the northern plains that have been imprinted by ancient impact basins (Isidis and Utopia). Just north of the boundary is the Elysium volcanic construct with grabens, surrounding wrinkle ridges and young Amazonian volcanics and channels. Elsewhere in the highlands are

Hesperian volcanics and the Hellas and Argyre impact basins. The volcanic areas are characterized by wrinkle ridges, and the dichotomy boundary by lobate scarps in the highlands and extensional structures towards the lowlands. Wrinkle ridges related to Tharsis loading are found throughout the lowlands of both hemispheres (Head *et al*., 2002; Tanaka *et al*., 2003).

2.2 Shape of Mars and crustal structure

The shape of Mars, consisting of the long-wavelength components of the topography, is to first order determined (1) by its global spin oblateness, (2) by a pole-to-pole slope that renders the northern hemisphere ∼5 km lower than the southern hemisphere (Smith *et al*., 1999b) and that is locally expressed by the highland–lowland dichotomy, and (3) by the topography of the Tharsis rise and any global-scale deformation induced by its attendant mass load (Phillips *et al*., 2001). The voluminous extrusive and intrusive magmatic deposits of Tharsis have loaded the lithosphere, leading to pervasive fracturing and folding over vast regions of the planet (Solomon and Head, 1982; Banerdt *et al*., 1992), and are responsible specifically for the radial extensional tectonic and concentric compressional tectonic features described earlier. Indeed, global-scale tectonics has been largely the result of the planetary response to Tharsis, plus the changing thermal state of the lithosphere. The Tharsis load has affected the shape of the planet by deforming the lithosphere as a thin spherical membrane, inducing the circumferential Tharsis flexural trough (surrounding moat) and contributing to high-standing topography in parts of Arabia Terra (the "Arabia bulge") (Phillips *et al*., 2001) (Plate 16). This global-scale deformation appears to control the azimuth of many Late Noachian valley networks, implying that most of the Tharsis mass was in place by the end of the Noachian period. This is consistent with the observation that over half of Tharsis-related extensional tectonic features are Noachian in age (Anderson *et al*., 2001). The Tharsis trough (surrounding moat) contains the vast majority of outflow channels on the planet (Phillips *et al*., 2001).

Bouguer gravity anomalies correlated with topography provided the first hard evidence that Mars has a distinct crust (Phillips *et al*., 1973), though such early analyses provided no information on mean crustal thickness or global crustal structure. Recent work has greatly improved our knowledge of crustal structure (Zuber *et al*., 2000; Zuber, 2001; Neumann *et al*., 2004, 2008). Geophysically, the mean crustal thickness has a lower bound of ∼50 km from the requirement that model Moho relief does not lead to negative crustal thickness anywhere on the planet (Zuber *et al*., 2000; Neumann *et al*., 2008). Using both geochemical and geophysical constraints, Wieczorek and Zuber (2004) find a mean crustal thickness of 50 ± 12 km. An upper bound on mean crustal thickness of ∼100 km results from

the constraint that Moho relief must be preserved against ductile collapse over billions of years (Nimmo and Stevenson, 2001; Zuber *et al*., 2000). Gravity/topography admittance estimates at the hemispheric dichotomy boundary yield an upper bound on crustal thickness of 75 km in that region (Nimmo, 2002).

Gravity and topography data show that crustal thickness is distinctly bimodal, with modal thicknesses of 32 and 58 km in the northern and southern hemispheres, respectively (Neumann *et al*., 2004). Regionally, the thickest crust is associated with the Tharsis volcanic construct, and the thinnest with major impact basins, such as Hellas, Argyre, and Isidis. Gravity and topography are both high on the Tharsis plateau and crustal thickness estimates here exceed 80 km at the higher elevations (Zuber *et al*., 2000; Zuber, 2001; Neumann *et al*., 2004, 2008).

The origin of the variation in crustal structure (the crustal dichotomy: the crustal expression of the global dichotomy) between the two hemispheres has been controversial. Given that the northern hemisphere crust beneath the Hesperian and Amazonian cover dates to the pre-Noachian (Frey *et al*., 2002; Frey, 2006a,b), global-scale crustal thickness variations could be a feature of primordial crustal fractionation, and the north–south crustal dichotomy must certainly predate the ancient impact basins Utopia and Hellas, whose Moho relief is preserved (Neumann *et al*., 2004). Global crustal thickness variations could also be due to a variety of other causes, including lower crustal flow induced by degree-1 convection (Wise *et al*., 1979; Zhong and Zuber, 2001; Roberts and Zhong, 2006) and very early plate tectonics (Sleep, 1994). The low elevation of the northern hemisphere could also be the result of one or more giant impacts (Wilhems and Squyres, 1984). By stripping away the cover of the Tharsis rise, Andrews-Hanna *et al*. (2008a) have shown that the global dichotomy boundary and lowlands have an elliptical shape, suggesting formation of the northern lowlands by a large oblique impact. Marinova *et al*. (2008) performed numerical simulations of single mega-impacts and found that for plausible impact energies, low impact velocities, and, in particular, impact angles in the 30–60° range, elliptical boundary shapes and basins similar to the shape found by Andrews-Hanna *et al*. (2008a) are achieved. For these models, the melt distribution stays within the impact basin and does not cover and obscure the dichotomy boundary.

2.3 Gravity field and lithospheric structure

Spectrally, the Tharsis rise and its global response largely account for (aside from the spin oblateness) the low-degree ($l \leq 10$) spherical harmonic gravity field and geoid of Mars. Spatially, the long-wavelength geoid of Mars (apart from its oblateness) is dominated by a strong anomaly (∼1000 m) centered on the Tharsis rise, a lesser high (∼500 m) over Arabia Terra (antipodal to Tharsis), and a negative

anomaly (∼−500 m) surrounding Tharsis (Smith *et al*., 1999b) (Plate 15). The last two features correspond to the antipodal Arabia bulge and the circumferential Tharsis trough discussed above (Plate 16). Shorter wavelength anomalies correspond to specific physiographic features (Lemoine *et al*., 2001), including the Valles Marineris, large shield volcanoes, and impact basins (notably Isidis and Utopia). The gravity anomalies are strong enough for most of these features to indicate a non-isostatic state and flexural support by the lithosphere (Zuber *et al*., 2000; McGovern *et al*., 2002, 2004b). The Utopia basin is unique in that it seems to support flexurally approximately 10 km (or more) of fill that has a large igneous component (Searls *et al*., 2006). Both the long- and short-wavelength gravity anomalies imply significant stress in the lithosphere; much of the tectonic fabric of the planet can be tied to these stresses, with the long-wavelength component, in turn, directly related to Tharsis.

The high-fidelity topographic information acquired by MOLA on the MGS mission, as well as the superb gravity field information derived from tracking the MGS, Mars Odyssey, and MRO spacecraft, have enabled a comprehensive survey of effective elastic lithosphere thicknesses (T_e) and from these estimates, the heat flow (Zuber *et al*., 2000; McGovern *et al*., 2002, 2004b; McKenzie *et al*., 2002; Belleguic *et al*., 2005; Milbury *et al*., 2007; Grott and Breuer, 2008; Phillips *et al*., 2008). Selected elastic thickness estimates are given in Table 5.1. Heat flow values are obtained from a yield-strength-envelope (Brace and Kohlstedt, 1980) analysis that equates the bending moment of an elastic lithosphere to that of a temperature-gradient-dependent elastic-plastic lithosphere (McNutt, 1984). These analyses show in general that with decreasing age, lithospheric loads were deforming increasingly thicker mechanical lithospheres. The implication is that heat flow declined rapidly during the Noachian, and, subsequently, more slowly; this is of course entirely consistent with both the exponential decrease in parent isotopes of heat-producing elements and the secular cooling of a terrestrial planet (e.g., Hauck and Phillips, 2002).

Most determinations of T_e have been derived in the spectral (wavelength) domain using gravity/topography admittance and correlation estimates (McGovern *et al*., 2002, 2004b; Belleguic *et al*., 2005). In the spatial domain, one or both of the gravity and topography data types have been used to estimate elastic thickness by comparing model stresses to fault locations circumferential to shield volcanoes and impact basins (Comer *et al*., 1985; Solomon and Head, 1990), and by analyzing linear fault deformation and rift flank uplift (Grott *et al*., 2005, 2007a; Kronberg *et al*., 2007). Phillips *et al*. (2008) used the lack of deflection of the substrate beneath the icy north polar cap load to derive a lower bound on present-day elastic thickness of 300 km. This implies that Mars has sub-chondritic heat sources, or that heat flow is regionally variable; for example, excess heat flow might be expected

Table 5.1. *Elastic lithosphere thicknesses through time on Mars*

Feature	Surface Age*	T_e, km
Olympus Mons[1,2]	A	>70, 93 ± 40
Ascraeus Mons[1,2]	A	2–80, 105 ± 40
Pavonis Mons[1]	A	<100
Arsia Mons[1]	A	>20
North Polar deposits[3]	A	>300
Alba Patera[1,2]	A–H	38–65, 66 ± 20
Elysium Rise[1,2,4]	A–H	15–45, 56 ± 20, 25–29
Solis Planum[1]	H	24–37
Hellas west rim[1]	H–N	<20
Coracis Fossae[5]	H–N	10–13
Hellas basin[1]	N	<13
Noachis Terra[1]	N	<12
Northeastern Terra Cimmeria[1]	N	<12
Northeastern Arabia Terra[1]	N	<16
Southern Thaumasia[6]	N	21–35
Acheron Fossae[7]	N	9–11

Selected elastic thickness (T_e) estimates from [1]McGovern *et al*. (2004b), [2]Belleguic *et al*. (2005), [3]Phillips *et al*. (2008), [4]McKenzie *et al*. (2002), [5]Grott *et al*. (2005), [6]Grott *et al*. (2007a), [7]Kronberg *et al*. (2007).
*A = Amazonian, H = Hesperian, N = Noachian.

in the Tharsis province, and, therefore, less than the planetary average elsewhere. Alternatively, in response to the polar load, the lithosphere might be in a transient state controlled by the viscosity of the mantle; however, this also implies sub-chondritic planetary heat sources.

2.4 Core, magnetic field, and true polar wander

Two-way ranging and Doppler tracking of the Mars Pathfinder lander yielded the first assumption-free estimate of the polar moment of inertia. This was done by estimating the precession rate of the rotational pole, which incorporated knowledge of the position of the Viking landers and derived pole 20 years earlier. The estimated polar moment of inertia of 0.3662 ± 0.0017 constrains the central metallic core to be between 1300 and 2000 km in radius (Folkner *et al*., 1997), though a reanalysis of the data lowers the moment of inertia to 0.3650 ± 0.0012 (Yoder *et al*., 2003). The estimate of the potential Love number k_2 of 0.153 ± 0.017 from MGS tracking constrains, under mild assumptions, the core radius to lie between 1520 and 1840 km, although these values would decrease somewhat if there is presently partial melt in the mantle (Yoder *et al*., 2003). The value of the Love number also

implies that the outer part of the core is liquid, consistent with the generation of a magnetic field early in Mars' history.

One of most startling discoveries of the MGS mission was that magnetic field mapping revealed the existence of strong remanent magnetic anomalies of various strengths, geometries, and locales (Acuña *et al*., 1999). The Terra Cimmeria region (in the Noachian southern highlands) (Plate 13) contains the strongest anomalies, and early interpretations of apparent alternating positive and negative quasi-linear zones of anomalies invoked a hypothesis for a plate-tectonics origin (Connerney *et al*., 1999), although the impression of linearity was aided by the choice of map projection. Other, weaker anomalies are scattered through the highlands, in the Tharsis region, and in the northern lowlands. The magnetic field information from MGS has gone through a number of data inversions that have improved the quality of the solutions (e.g., Purucker *et al*., 2000; Arkani-Hamed, 2001; Langlais *et al*., 2004; Hood *et al*., 2005). Mitchell *et al*. (2007) used electron reflectometry data from MGS to produce a nearly global map of the magnetic field that resolved anomalies about seven times weaker than determinations from the MGS magnetometer. Numerous small anomalies are found in the northern lowlands, suggesting that the northern crust was at one time more magnetized than at present. In particular, the anomalies ring, but do not occur in, the Utopia basin, supporting the view that this feature was formed subsequent to the dynamo die-off, as proposed by Frey (2006b). Additionally, the area immediately to the north of the Tharsis rise is devoid of magnetic anomalies, suggesting a thermal demagnetization connection to this massive volcanic province (Mitchell *et al*., 2007).

Collectively, the magnetic field anomalies require that Mars had a global-scale internal field early in its history, but the origin of the spatial distribution of the anomalies and the timing of the internal dynamo remain as unsolved problems (Solomon *et al*., 2005). Although other interpretations are possible, the most likely reason for the absence of magnetic field anomalies over the Hellas and Argyre basins is that the dynamo had ceased to exist by the time these basins had formed. Magnetization lost by the high interior temperatures and shock associated with the impact would not have been reacquired. Tighter bounds on dynamo extinction in the pre-Noachian are estimated by the crater ages of large impact basins (some are QCDs) that are spatially associated with varying strengths of crustal magnetic fields (Frey, 2006b).

Of particular interest to the tectonics of Mars is the presence of magnetic anomalies high on the Tharsis rise (Johnson and Phillips, 2005). Either these anomalies were acquired by cooling Tharsis magmas when the dynamo was active, or they are in older basement that was uplifted during the formation of Tharsis. If the magnetic field ceased by the time Hellas/Argyre formed, then the former hypothesis requires that the Tharsis origin dates back to the earliest Noachian. These anomalies on

Tharsis are not found in the highest parts of the rise or in the vicinity of the large shield volcanoes (Tharsis Montes), suggesting thermal demagnetization has been an important process (see also Mitchell *et al*., 2007). Jellineck *et al*. (2008) used the presence and scale of the Tharsis demagnetized region as a constraint on geodynamical properties of the regional interior, deriving a Noachian elastic thickness range of 29–40 km, excess mantle temperature of 205–240 °C, and a plume heat flux of 60–100 mWm^{-2}.

The plethora of magnetic field models from the MGS mission data has led to estimates of magnetic paleopole locations by determining the vector magnetization direction of isolated remanent magnetic anomalies and assuming that the global magnetic field was dominated by the dipole term. Such an exercise should be approached cautiously because of the non-uniqueness of potential field inversions, unknown causative body geometry, and the likely poor resolution of distinct sources at MGS altitudes (Langlais *et al*., 2004; Biswas and Ravat, 2005). Estimated paleopole locations have been all over the map, with the most consistent results showing paleopole locales in the vicinity of the Tharsis rise (Arkani-Hamed and Boutin, 2004; Hood *et al*., 2005; Quesnel *et al*., 2007). If the magnetic pole was always close to the rotational pole, then magnetic paleopoles that do not coincide, more or less, with the present spin axis imply that Mars has undergone true polar wander (Melosh, 1980; Willemann, 1984; Zuber and Smith, 1997; Sprenke *et al*., 2005; Matsuyama *et al*., 2006; Roberts and Zhong, 2007). If this is so, then the most likely suspect is the growth of Tharsis, which if not already on the equator, would migrate there via true polar wander to maintain rotational stability of the planet.

True polar wander has been a contentious topic for Mars. The geologic evidence for true polar wander is ambiguous at best (Banerdt *et al*., 1992, and references therein). The long-wavelength structures in the proposed shorelines of putative northern lowlands oceans (itself a contentious topic and beyond the scope of this review) are consistent with the deformation expected from a post-Tharsis loading true polar wander event, though the source of the driving mass is unclear (Perron *et al*., 2007). However, on Mars, true polar wander sets up large stress fields (Melosh, 1980) and well-defined tectonic patterns from moving the lithosphere over the equatorial (spin) bulge, which have not been observed (Grimm and Solomon, 1986). These tectonic features likely should have been preserved at least on post-Tharsis Mars, and possibly even from the proposed Tharsis true polar wander event itself.

3 Tectonic features

3.1 Extensional structures

Extensional structures identified on Mars include very narrow cracks or joints to fairly narrow linear negative relief structures (grabens that are a few kilometers

wide and of order hundred meters deep) to enormous troughs and rifts that are up to 100 km wide and several kilometers deep (see review by Banerdt *et al*., 1992 and references therein). Most interpretations of the grabens and rifts suggest they are bounded by steeply dipping normal faults whose strike is generally perpendicular to the least compressive principal stress. Large troughs and rifts (Plates 17 and 25) are likely bounded by relatively high-angle normal faults that cut through the entire brittle lithosphere (Frey, 1979; Schultz, 1991, 1995; Mege and Masson, 1996b; Anderson and Grimm, 1998; Hauber and Kronberg, 2001, 2005; Wilkins and Schultz, 2003; Grott *et al*., 2007b).

Viking images of narrow grabens show fairly fresh looking fault scarps and flat floors suggesting simple structures. Photoclinometry on Viking images and MOLA data show the scarps overall have extremely low slopes ($\sim 9^\circ$) (Davis *et al*., 1995; Golombek *et al*., 1996; Harrington *et al*., 1999) and high-resolution MOC images show evidence for significant erosion and deposition within the structures, which could conceal a more complex subsurface structure (Figure 5.1a and b). Bounding faults that dip inward at $\sim 60^\circ$ would intersect at depths of several kilometers (Tanaka and Golombek, 1989; Davis and Golombek, 1990), which could represent a mechanical discontinuity (Tanaka *et al*., 1991; Thomas and Allemand, 1993; Davis *et al*., 1995; Borraccini *et al*., 2006). The faults could extend below their intersection depths in hourglass structures or one fault could terminate against a master fault that extends to greater depth (Schultz *et al*., 2007). Alternatively, dikes could underlie the normal faults and accommodate the strain at greater depth (Schultz *et al*., 2004; Goudy and Schultz, 2005). The association of narrow grabens and tension cracks with volcanic flows, pit chains and outflow channels is well documented for certain areas (Tanaka and Golombek, 1989; Tanaka and Chapman, 1990; Burr *et al*., 2002a,b; Hanna and Phillips, 2006), although not always in the same area as most pit crater chains do not show associated volcanics (Ferrill *et al*., 2004; Wyrick *et al*., 2004). Subsequent work has argued that most, if not all grabens are the surface manifestations of subsurface dikes (Mege and Masson, 1996a; Ernst *et al*., 2001; Scott and Wilson, 2002; Scott *et al*., 2002; Wilson and Head, 2002) and that massive dikes could underlie Valles Marineris troughs and be responsible for the associated catastrophic outflow channels (McKenzie and Nimmo, 1999). Mege *et al*. (2003) have further argued that multiple dikes or dike swarms underlie each graben based on terrestrial analogues and experimental extension and deflation experiments. Analysis of the occurrence, size, and characteristics of pit crater chains associated with grabens on Mars argues that most are not volcanogenic, however, but are rather related to dilational normal faulting (Ferrill *et al*., 2004; Wyrick *et al*., 2004). Regardless of what happens to the faults beneath narrow grabens on Mars, their relief suggests they accommodate small amounts of extension (order 100 m or less) and strain (locally $<10\%$).

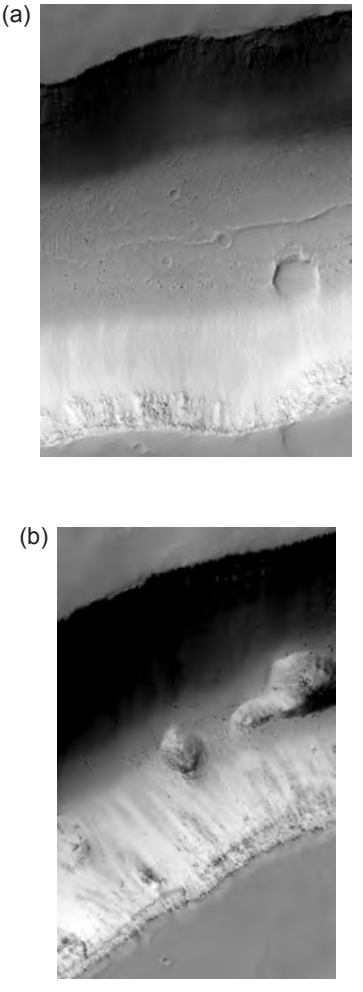

Figure 5.1. High-resolution (1.4 m/pixel) MOC narrow-angle images of grabens on Mars showing highly modified appearance. (a) 3-km wide graben in Memnonia Fossae (MOC image M02-02352 is 2.9 km wide; north is roughly up). (b) 2-km wide graben in Sirenum Fossae (MOC image M02-04357 is 1.4 km wide; north is roughly up). Both grabens have steep upper walls ($\sim$30°) with exposures of rock and lower walls with no rocks apparent, suggesting deposition of fine-grained material. Both floors are littered with boulders $\sim$1.5 to 15 m in diameter that likely eroded from the upper walls. Deposition of sediment is apparent by eolian bedforms in (a), suggesting deposition of eolian material and downward streaks in (b). Although the floor of (a) is reasonably flat, the floor of (b) includes mounds of material that could be wall rock and or interior hanging wall remnants of a complex interior structure. The highly modified floor and walls make inferences about the geometry of the structure difficult and allow a complexly faulted downthrown block that is covered up by sediment.

3.2 Compressional structures

Wrinkle ridges are the most common compressional structures on Mars and are composed of linear to arcuate asymmetric ridges hundreds of meters high, up to a few tens of kilometers wide, and can be hundreds of kilometers long (Plate 18). They are commonly evenly spaced and typically have a small crenulation or surface wrinkle and a broad rise adjacent or as part of the feature. Initial work on lunar wrinkle ridges suggested origins relating to both volcanic and tectonic processes, but more recent work consistently argues that these features are compressional structures that involve thrust faulting and folding (e.g., Plescia and Golombek, 1986; Mueller and Golombek, 2004). Detailed analysis and modeling of MOLA topography and comparison to compressional structures on Earth has shown that many aspects of wrinkle ridges are consistent with surface folding overlying blind thrusts at depth (e.g., Schultz, 2000; Golombek *et al*., 2001; Vidal *et al*., 2003; Mueller and Golombek, 2004). In this interpretation, slip on the underlying thrust fault is accommodated by asymmetric flexural slip folding in strong, but weakly bonded, layered materials (volcanics or sedimentary rocks) near the surface and thus wrinkle ridges represent fault-propagation folds (e.g., Suppe and Medwedeff, 1990) or trishear fault-propagation folds (Erslev, 1991) (Figure 5.2). The asymmetric fold shape with steep forelimbs and shallow backlimbs of these structures are consistent with thrust faults that dip beneath the shallow backlimb. Smaller crenulations are likely high-level backthrusts that nucleate at weak layers in the upper crust or by flexural slip folds that facilitate bending of layered materials (Schultz, 2000; Okubo and Schultz, 2003, 2004; Mueller and Golombek, 2004). A variety of kinematic and dynamic models show that the relief of the ridge (hundreds of meters) is a measure of the shortening, and that wrinkle ridges accommodate very small amounts of shortening (order 100 m) and strain (of order 0.1% or less) (Watters, 1988, 2004; Golombek *et al*., 1991; Plescia, 1991a, 1993; Schultz, 2000; Golombek *et al*., 2001).

Lobate scarps (Figure 5.3) and other large ridges also have been identified on Mars (Chicarro *et al*., 1985; Watters, 1993, 2003b; Schultz and Tanaka, 1994; Watters and Robinson, 1997; Watters *et al*., 2000; Anguita *et al*., 2001, 2006; Grott *et al*., 2007a). These structures are larger (hundreds of meters to several kilometers high) and have been inferred to represent lithospheric scale thrust faults in heavily cratered Noachian terrain (Schultz and Tanaka, 1994). Displacement–length ratios for the lobate scarps (Watters, 2003b) are much greater (10 times) than wrinkle ridges (Tate *et al*., 2002b; Mueller and Golombek, 2004), but still about an order of magnitude smaller than for typical thrust faults on Earth (Watters and Robinson, 1997; Watters *et al*., 2000; Watters, 2003b). The morphology of these ridges is characterized by fairly simple linear to arcuate (lobate), asymmetric

Figure 5.2. High-resolution MOC image (5.6 m/pixel) showing well-preserved detailed structure of wrinkle ridge. Note surface fold with narrow (25–100 m wide) extensional structures along the crest, likely generated in response to bending stresses over the fold (e.g., Mueller and Golombek, 2004; Plescia and Golombek, 1986). Eolian bedforms deposited at the base of the structure partially cover the crenulations. Similar surface texture and preservation of fine scale structures suggest that total modification of the structure has been relatively modest. MOC image E05-01229 is 2.9 km wide, north is roughly up.

scarps (Figure 5.3), suggesting a simple subsurface thrust fault that actually breaks the surface (or in which folding of surface layers is less important) (Vidal *et al*., 2005). In certain cases, wrinkle ridges change along-strike to lobate scarps, coincident with a change from smooth layered materials to highlands material (Watters, 1993). Based on the relief of lobate scarps, shortening is estimated to be hundreds of meters to kilometers, which is substantially greater than wrinkle ridges.

Although most workers agree that lobate scarps and other large ridges likely represent thrust faults that extend through most, if not all of the brittle lithosphere (Schultz and Tanaka, 1994), there is no such agreement on the depth of penetration of faults beneath wrinkle ridges. Thin-skinned deformation has been argued to explain the regular spacing (Plate 18) of wrinkle ridges (buckle folds in a thin

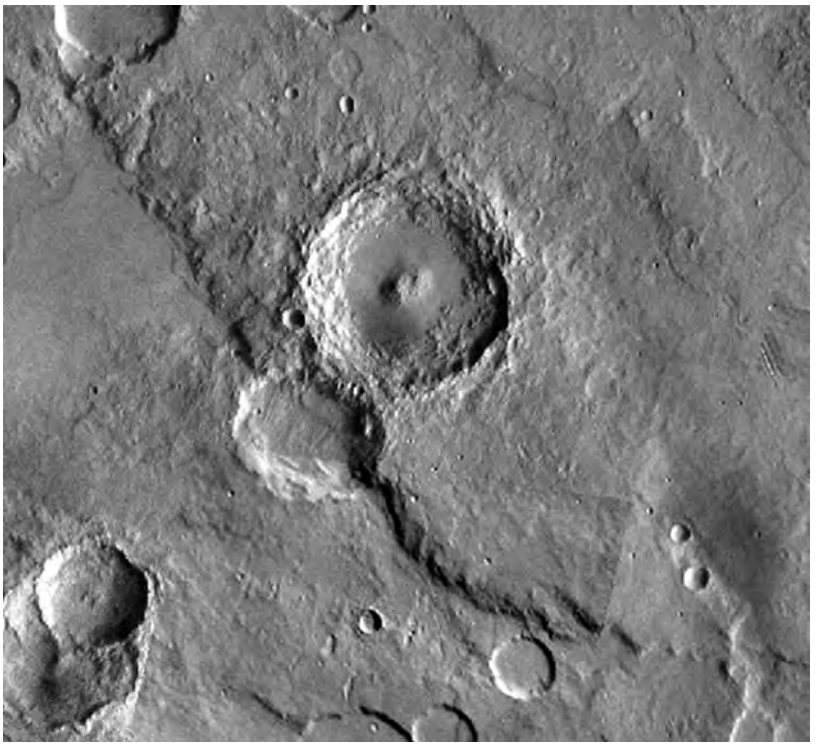

Figure 5.3. Viking mosaic of lobate scarp Amenthes Rupes, interpreted to be a thrust fault that breaks the surface of Mars. This large lobate scarp with over 1 km of relief and a shortened impact crater suggests several kilometers of shortening on a shallowly, northeastward dipping thrust fault (Vidal *et al*., 2005). Mars Digital Image Mosaic is ∼500 km wide centered at 111°E, 2.5°N; north is up.

strong layer) and the abrupt change in wrinkle-ridge trend around the rims of some craters (suggesting a shallow fault and/or décollemont) (Watters, 1991, 2004; Allemand and Thomas, 1995; Mangold *et al*., 1998). Thick-skinned deformation in which subsurface faults extend through most or all of the lithosphere is based on observed elevation offsets and stair step topography across some adjacent wrinkle ridges, suggesting they are underlain by stacked thrust faults and the mechanical difficulty in preventing the strain observed at the surface from being accommodated by faulting at deeper levels (Zuber and Aist, 1990; Golombek *et al*., 1991, 2001; Zuber, 1995; Montesi and Zuber, 2003; Mueller and Golombek, 2004).

3.3 Strike-slip faults

Strike-slip faults are uncommon on Mars (and other single plate planets) (Golombek, 1985; Tanaka *et al*., 1991; Banerdt *et al*., 1992) and typically are found

as accommodation structures associated with wrinkle ridges and compressional push ups (Schultz, 1989; Watters, 1992; Anguita *et al*., 2001, 2006) or associated with radial graben and concentric wrinkle ridges to the west of Tharsis (Okubo and Schultz, 2006; Andrews-Hanna *et al*., 2008b). Ancient strike-slip faults of lithospheric proportion also have been proposed (Forsythe and Zimbelman, 1988).

4 Tectonic history, orientation and distribution of structures

The broad pattern of deformation in the western hemisphere is dominated by the giant radiating pattern of extensional structures and the sweeping family of compressional ridges and wrinkle ridges associated with Tharsis (Wise *et al*., 1979; Anderson *et al*., 2001). Structures around Tharsis are not uniformly distributed, but are found concentrated in particular regions separated by areas with different types of structures or no apparent deformation. Detailed mapping in these deformed regions, which have rich stratigraphies (Scott and Tanaka, 1986; Tanaka and Davis, 1988; Tanaka, 1990; Scott and Dohm, 1990a,b; Witbeck *et al*., 1991; Morris and Tanaka, 1994; Dohm and Tanaka, 1999; Dohm *et al*., 2001), has revealed a complex deformational history that has spanned most of the preserved geologic record on Mars. This detailed mapping has been pieced together at a global scale (Plate 24 in Tanaka *et al*., Chapter 8) to provide a record of the deformation through time on Mars (Anderson *et al*., 2001, 2004, 2008; Tanaka *et al*., Chapter 8). We will first briefly describe the deformed regions and then the global tectonics.

4.1 Alba Patera and Ceraunius Fossae

North of the Tharsis Montes and their associated Amazonian volcanic cover are heavily faulted Noachian terrains of Ceraunius Fossae, and to the north, the Amazonian volcano Alba Patera (Plate 13). Ceraunius Fossae is composed of closely spaced narrow grabens and fault scarps that formed mostly during the Late Noachian and Early Hesperian (Tanaka, 1990). Deformation towards the north in the younger Hesperian and Amazonian volcanics appears to splay around Alba Patera, extending into the northern plains, with most extensional structures on the eastern side (Scott and Wilson, 2002; Cailleau *et al*., 2003, 2005; Ivanov and Head, 2006). Grabens here are wider than most (2–8 km) with complex fault scarps and shallow, relatively flat floors a few hundred meters deep (Plescia, 1991a). Most of these structures formed in the Early Amazonian, although deformation continued into the Middle to Late Amazonian concentrated on regularly spaced, wider and deeper complex grabens with pit chains along their axes (Tanaka, 1990). A transect across the southern part of Alba at 35°N, in which the depth of grabens and fault scarps was measured from shadows and photoclinometry, yielded a total

extension of about 8 km for assumed normal fault dips of 60° (Plescia, 1991a). Strain estimates vary from ∼5% across individual structures to ∼0.5% across the entire ∼1500 km transect.

Measurement of the displacement across Ceraunius Fossae, just south of the above transect, in stacked MOLA profiles yields much larger extensions of 36 km and 42 km (Borraccini *et al*., 2005), which correspond to about 2% strain across the entire region. The factor of five difference in extension between the two estimates that cross similar concentric sectors may be related to the older age of Ceraunius Fossae basement (Noachian), and so may be recording more extension compared with the Amazonian transect through Alba.

4.2 Structures associated with volcanoes

The large volcanoes of Tharsis, Olympus Mons, Arsia Mons, Pavonis Mons, Ascraeus Mons and Alba Patera, also have locally associated structures (Crumpler and Aubele, 1978; McGovern and Solomon, 1993). All have central calderas likely related to shallow magma chambers (Mouginis-Mark, 1981; Zuber and Mouginis-Mark, 1992; Crumpler *et al*., 1996), most have fissure and flank rift structures, often in preferred directions (Crumpler and Aubele, 1978), and many have peripheral circumferential normal faults and grabens that have been related to local lithosphere flexure due to loading (Comer *et al*., 1985; McGovern and Solomon, 1993), edifice spreading (McGovern and Solomon, 1993), and dike or sill intrusion (Scott *et al*., 2002; Cailleau *et al*., 2003, 2005; Ivanov and Head, 2006). Many of the grabens and flank structures have pits along their floors and end in sinuous rilles and channels, suggesting that they are underlain by volcanic dikes (Tanaka and Golombek, 1989; Ernst *et al*., 2001; Wilson and Head, 2002; Mege *et al*., 2003). Calderas are bounded by large normal faults that have accommodated kilometers of slip down to caldera floors that can have smaller parallel graben and radial wrinkle ridges. Compressional deformation on the higher flanks of the volcanoes has been suggested (Thomas *et al*., 1990; McGovern and Solomon, 1993), as has folding of the flanks from the weight of the volcanic mass (Borgia *et al*., 1990). Disrupted aureole deposits (Harris, 1977) and a large scarp around Olympus Mons have been interpreted as due to landslide deposits from gravity sliding headed by listric normal faults (Lopes *et al*., 1980, 1982; Francis and Wadge, 1983; Tanaka, 1985; McGovern *et al*., 2004a).

4.3 Tempe Terra

To the east of Alba Patera and northeast of (and in line with) the Tharsis Montes is Tempe Terra (Plate 13), a plateau of Noachian through Hesperian terrain that

borders the northern plains to the north–northeast. Tempe has a complex faulting history with a peak in northeast trending grabens and normal faults in the Middle–Late Noachian to Early Hesperian and in the Late Hesperian (Scott and Dohm, 1990a,b; Moore, 2001; Fernández and Anguita, 2007). Most of the structures in Tempe Terra are fairly narrow grabens, but large rifts of Tempe Fossae (Plate 25) are analogous to large continental rifts on Earth (Hauber and Kronberg, 2001). Northwest striking wrinkle ridges are found on Hesperian ridged plains that appear to extend north from Lunae Planum. Extension across Tempe Terra has been estimated from shadow and fault scarp widths and deformed craters (Golombek *et al*., 1996) to be about 22 km across two ∼1000 km traverses (regional strain of ∼2%). MOLA elevation profiles indicate lower scarp slopes across the rifts (Harrington *et al*., 1999) consistent with measurements by Hauber and Kronberg (2001) of the large rifts and indicate the total extension across Tempe Terra is probably slightly lower (roughly 20 km).

4.4 Lunae and Solis Plana

South of Tempe Terra and to the east and southeast of the Tharsis Montes are the classic wrinkle ridge provinces of Lunae and Solis Plana (Plate 13). Wrinkle ridges on Tempe, Lunae and Solis define a sweeping roughly concentric system to Tharsis (Wise *et al*., 1979; Maxwell, 1982; Watters and Maxwell, 1986; Anderson *et al*., 2001). Ridges are larger and more widely spaced on Solis Planum than Lunae Planum (Watters, 1991; Golombek *et al*., 2001). These areas are mapped as Hesperian ridged plains (Scott and Tanaka, 1986), interpreted to be underlain by layers of flood basalts totaling several kilometers thick (e.g., Watters, 1991). MOLA elevations indicate some ridges in Solis Planum accommodate adjacent stair step offsets in elevation, suggesting a package of stacked west-dipping underlying thrust faults that root in the ductile lower crust and are analogous to small foreland basement uplifts on Earth (Golombek *et al*., 2001; Montesi and Zuber, 2003). Estimates of radial shortening across Lunae Planum (Plate 18) suggest very low regional strain of 0.1–0.3% (Golombek *et al*., 1991; Plescia, 1991b; Tate *et al*., 2002a,b). The compressional deformation that formed the wrinkle-ridges appears coeval for all of the wrinkle-ridge provinces and is constrained globally to have been dominantly in the Hesperian (Scott and Dohm, 1990b; Mangold *et al*., 2000), although some formed in the Late Noachian and Early Amazonian (Chapter 8; Tanaka *et al*., 1991, 2003, 2005).

4.5 Valles Marineris and Noctis Labyrinthus

Separating Lunae and Solis Plana is the great rift of Valles Marineris (Plate 13), which is composed of troughs that are up to 10 km deep, tens to hundreds of

kilometers wide, and many hundreds to a thousand kilometers long. The formation of Valles Marineris began in the Late Noachian–Early Hesperian with faulting, broad basin formation and subsequent major trough formation (Witbeck *et al*., 1991; Lucchitta *et al*., 1992; Peulvast and Masson, 1993a,b; Schultz, 1998). Younger deposits and landslides within the troughs are Amazonian in age, and collapse of Noctis Labyrinthus troughs occurred in the Late Hesperian–Early Amazonian (Tanaka and Davis, 1988). The origin of Valles Marineris as a large rift is based on the identification of large fault scarps along the base of the chasmata, mapped downdropped blocks, structural models, and orientation radial to Tharsis (Lucchitta *et al*., 1992; Peulvast and Masson, 1993a,b; Anderson and Grimm, 1998; Schultz, 1998; Schultz and Lin, 2001; Wilkins and Schultz, 2003). Extension across the central portion of Vallis Marineris from relief and structural offsets (that account for deposition within the troughs) varies between 10–60 km (20–30 km for 60° dipping faults) (Schultz, 1995; Mege and Masson, 1996b). Strain varies from ∼20% across the individual chasmata to about 0.6% if measured across the entire shadow region (without extensional deformation) to the next extensional fault terrains (Tempe to Thaumasia) radial to Tharsis.

4.6 Claritas Fossae, Thaumasia, and Sirenum

South of the Tharsis Montes and west of Syria Planum is a high standing ridge of highly fractured terrain known as Claritas Fossae, which extends farther south into Thaumasia (Plate 13). This ridge of Noachian terrain continues in an arc south and to the east, where it joins the Coprates rise, south of Coprates Chasma. It is on-lapped by Hesperian plains to the north and records a well-preserved sequence of structural events (Dohm and Tanaka, 1999; Dohm *et al*., 2001). The southern margin of the ridge itself is likely a thrust associated with Tharsis (Courtillot *et al*., 1975; Masson, 1977; Wise *et al*., 1979) and appears related to a series of Noachian lithospheric buckles and thrusts that are roughly concentric to Tharsis and extend in an arc from Coprates through Thaumasia to Terra Sirenum and Memnonia (Schultz and Tanaka, 1994; Anguita *et al*., 2001, 2006; Grott *et al*., 2007a). Claritas Fossae is dominated by generally north striking normal faults and grabens that continue south into Thaumasia. The Thaumasia rift (Hauber and Kronberg, 2005) is part of Claritas Fossae and is roughly 100 km wide and several kilometers deep (Plate 17). Similar size rifts (Coracis Fossae) are found in the Thaumasia, highlands to the southeast (Grott *et al*., 2007b). A distinct fanning set of grabens radiates to the south, and southeast into Thaumasia, and to the southwest and west in Sirenum (Borraccini *et al*., 2007).

Detailed mapping has established multiple faulting episodes (Dohm and Tanaka, 1999; Dohm *et al*., 2001) with first Claritas faulting occurring in the Early to Middle

Noachian with a series of east–west (Tharsis-circumferential) trending fault scarps (Tanaka and Davis, 1988), which may record the earliest structural uplift of Tharsis (Phillips *et al*., 1990; Johnson and Phillips, 2005). Subsequent faulting events occurred in the Late Noachian–Early Hesperian (NE trending structures, including Coracis Fossae), with the fanning set forming in the Early Hesperian (Anderson *et al*., 2001). Estimates of extension across the Thaumasia rift in Claritas and both Coracis Fossae rifts in Thaumasia to the southeast from MOLA topography are 1–4 km (Hauber and Kronberg, 2005) and 2–2.5 km (Grott *et al*., 2007b), respectively, assuming 60° dipping normal faults. Measurements of fault scarp widths and shadows across grabens of Thaumasia and southern Claritas, and Sirenum yield extension estimates of about 11 km and 3 km, respectively (Golombek *et al*., 1994; Golombek *et al*., 1997). If the rift extensions in Claritas and Coracis Fossa are added, the total extension across the Thaumasia region could be as high as 18 km assuming displacement across 60° dipping normal faults.

4.7 Western hemisphere tectonic history

Placing the mapping results of the geologic and tectonic activity within these deformed regions into the global stratigraphic framework of Mars (Tanaka, 1986) has revealed a complex structural history involving five main stages of tectonic activity in the western hemisphere, with distinct centers of tectonic activity through time (Anderson *et al*., 2001). Careful testing of the geometry of all structures in the western hemisphere shows statistically significant radial (extensional) and concentric (compressional) orientations about the highest standing portion of Tharsis (excluding the volcanoes) near Syria Planum (Anderson *et al*., 2001). More than half of the structures mapped on Mars are Noachian in age (stage 1; >3.8 Ga), concentrated in exposures of Noachian age crust in Tempe Terra, Ceraunius Fossae, Syria Planum, Claritas Fossae, Thaumasia, and Sirenum (see Plate 24). About half of these grabens are radial to a center of activity in Claritas Fossae, the ancient Noachian ridge west of Syria. By Late Noachian–Early Hesperian (stage 2), activity was concentrated in Thaumasia and Valles Marineris. Early (to Late) Hesperian (stage 3) included the development of concentric wrinkle ridges concentrated along the edge of the topographic rise, in the northern plains and in volcanic provinces in the eastern hemisphere. Normal faulting also occurred north of Alba, in Tempe Terra, in Ulysses Fossae, in Syria Planum and Valles Marineris, and in Claritas Fossae and Thaumasia. Stage 3 structures are generally radial (grabens) or concentric (wrinkle ridges) to Syria Planum. Stage 4 activity during the Late Hesperian–Early Amazonian was concentrated in and around Alba Patera and Middle to Late Amazonian activity (stage 5) was concentrated in and around the Tharsis Montes volcanoes.

Given that about half of all extensional structures preserved in the western hemisphere formed before the Late Noachian, Tharsis tectonic activity peaked early and decreased with time. The observation that Noachian through Amazonian radial grabens and concentric wrinkle ridges formed, centered at slightly different locations (local centers of volcanic and tectonic activity) within the present-day highest standing terrain of Tharsis, indicates that the basic lithospheric structure of the western hemisphere has changed little since the Middle Noachian (Anderson *et al*., 2001). This result is in agreement with geophysical results discussed below.

4.8 Eastern hemisphere

Elysium is a smaller volcanic province than Tharsis (Mouginis-Mark *et al*., 1984) with some surrounding structures and a small, elevated plateau with a thickened crust (Neumann *et al*., 2004). Elysium Mons (Plate 13), the largest shield volcano in the province, is similar to the giant Tharsis shield volcanoes, with a central caldera and peripheral concentric grabens and normal faults attributed to loading (Comer *et al*., 1985). Cerberus Fossae, southeast of Elysium Mons, trend east–southeast and appear radial to Tharsis (Hall *et al*., 1986) and north- to northeast-trending wrinkle ridges in Elysium and Arcadia Planitae may be concentric to Tharsis. Cerberus Rupes have been reactivated repeatedly and are the source of very young volcanism and fluids forming the channels and volcanic plains of Athabasca and Marte Valles (Burr *et al*., 2002a,b; Jaeger *et al*., 2007). Other extensional grabens (Plate 24) appear radial to Elysium (Anderson *et al*., 2008). Wrinkle ridge formation in Arcadia formed on a thin ridged plains unit in the Late Hesperian (Tanaka *et al*., 2005), coeval with other ridged plains, and the compressional strain has been estimated to be ∼0.06% across a ∼1000 km transect (Plescia, 1993).

Hesperia Planum, Syrtis Major Planum (Plate 13) and other plains (possibly volcanic) regions in Arabia Terra also have populations of wrinkle ridges in the eastern hemisphere (Anderson *et al*., 2008). Wrinkle ridges in Hesperia Planum form a reticulate pattern with northeast and northwest trending sets (Raitala, 1988; Goudy and Schultz, 2005). Wrinkle ridges in Syrtis Major show radial and concentric patterns (Hiesinger and Head, 2004). Circular rings of ridges are also found, suggesting their trends are guided by subsurface shallowly buried craters (Raitala and Kauhanen, 1989; Allemand and Thomas, 1995). Both the ridges and plains formed in the Hesperian (Scott and Dohm, 1990b; Watters, 1993; Mangold *et al*., 2000) (Plate 24).

Structures in the eastern hemisphere are also associated with the large basins: Isidis, Utopia and Hellas (Plate 13). Isidis has concentric grabens still preserved in Noachian crust to the northwest and southeast, and Hellas has extensional structures preserved to the west at distances that have been related to mascon loading (Comer *et al*., 1985; Wichman and Schultz, 1989). The structures are Late

Noachian–Early Hesperian in age (Wichman and Schultz, 1989; Tanaka and Leonard, 1995; Leonard and Tanaka, 2001). Concentric grabens have not been recognized at Utopia. Ridges within the Isidis and Utopia basins, recently discovered in MOLA data (similar to those in the northern plains, see next section), are numerous, showing a complex radial and concentric pattern (Thomson and Head, 2001; Head *et al*., 2002; Tanaka *et al*., 2003), suggesting that stresses related to basin subsidence may be important (although finite-element elastic modeling of Utopia basin does not support this view (Searls and Phillips, 2007)). Fewer ridges are present in Hellas, although they tend to be radial. The ridges have been interpreted as wrinkle ridges formed from compressional deformation and are Early Hesperian in age, although reactivation may have occurred in Early and Middle Amazonian (Tanaka *et al*., 2005).

The dichotomy boundary in the eastern hemisphere is characterized by scarps and troughs aligned with the boundary that were proposed to represent Late Noachian–Early Hesperian normal faulting that accommodated the lowering of the northern plains (Maxwell and McGill, 1988; McGill and Dimitriou, 1990; Smrekar *et al*., 2004). As discussed earlier, it is very likely that the northern lowlands crust dates from the pre-Noachian (Frey *et al*., 2002; Nimmo and Tanaka, 2005; Frey, 2006a,b). Therefore, the scarps and troughs likely represent a later southward retreat of the dichotomy boundary, which originally may have been sharpened by faulting (Guest and Smrekar, 2005), but then may have been eroded by fluvial processes during a period of "wet" climate that occurred during the Noachian–Hesperian transition (Howard *et al*., 2005; Irwin *et al*., 2005).

Lobate scarps trend parallel to the boundary (Watters, 2003a) and formed in the Late Noachian, roughly coeval with the Noachian ridge belt south of Tharsis (Schultz and Tanaka, 1994). The topography of adjacent highlands in the Amenthes region rises to a crest up to 1 km above its surroundings over a distance of 200 km away from the margin, suggestive of a passive margin (Frey *et al*., 1998) or flexed elastic plate (Watters, 2003a). Bending stresses in a simple, broken flexed plate, subject to a vertical load and bending moment at the broken end, would be extensional over the crest where the compressional lobate scarps are found, suggesting that erosional and/or global stresses may be important in the formation of the lobate scarps (Watters, 2003a,b). Alternatively, a faulted plate model with finite extension and specified fault dip will generate compressional stresses in the footwall and extensional stresses in the hanging wall (Weissel and Karner, 1989). This is consistent with observations and may obviate the need for global compressional stresses for the formation of these lobate scarps; footwall compressional stresses in this case would be amplified by erosion of the footwall block. Alternatively, Nimmo (2005) has shown that lower crustal flow leads to differential thickness changes north and south of the dichotomy boundary, correctly predicting faulting styles.

4.9 Northern plains

Not seen in generally poor, high latitude Viking images, an extensive system of ridges in the northern plains was discovered in the MOLA topographic data (Withers and Neumann, 2001). The height, width, length, organized pattern and spacing of the ridges resemble wrinkle ridges found on the classic ridged plains. In addition, the ridges continue in the northen plains in a large concentric arc between Tempe Terra and Arcadia Planitia (Plates 13 and 24), suggesting they are produced by radial compressive stresses from Tharsis (Withers and Neumann, 2001). In general, ridges on the northern plains appear to have lower relief and a more rounded appearance (less crenulated), suggesting partial burial (Head *et al*., 2002) and/or formation in layered materials (sediments) of different rheology (Tanaka *et al*., 2003, 2005). The wider spacing of the ridges in the northern plains has been attributed to burial (Head *et al*., 2002) or to a thinner crust resulting in a greater brittle–ductile transition depth, which controls fault spacing (Montesi and Zuber, 2003). Constraints on the timing of formation appear consistent with the global period of wrinkle ridge compression in the Hesperian (Head *et al*., 2002; Tanaka *et al*., 2003) and perhaps continued regional compression in the northern plains into the Amazonian (Tanaka *et al*., 2005).

5 Tharsis geodynamical models and comparisons to tectonics

5.1 Models for the origin of Tharsis

Two general models have been proposed to explain the gravity field and topography associated with Tharsis that bear on the origin of this planetary-scale feature: elastic spherical shell loading (Banerdt *et al*., 1982, 1992) and plume uplift with the attendant deformation of the lithospheric shell. Elastic spherical shell loading models propose that whatever the origin of Tharsis, by the end of the Noachian, mechanically Tharsis was a massive load supported largely by membrane stresses in a rigid lithosphere. Further, this mass distribution has changed little since that time. Plume models posit that the long-wavelength topography of Tharsis is presently supported to a significant fraction by a plume, and that plume-related radial subsurface dikes are responsible for the radial graben system (Mege and Masson, 1996a; McKenzie and Nimmo, 1999; Ernst *et al*., 2001; Wilson and Head, 2002). Such models can be consistent with the observed degree two and three (and higher) topography and gravity fields (Kiefer *et al*., 1996), but lack the overwhelming success in predicting the style and distribution of stress and strain predicted by elastic shell loading models (see below).

The challenge to plume models for Mars is to generate but a single plume to create Tharsis (and possibly a second plume to create Elysium). In a series

of papers, Harder (1998, 2000) and Harder and Christensen (1996) show that if the mantle endothermic spinel–perovskite phase transition exists just above the Martian core, then only a few plumes are generated in the mantle (with time, only one), and that about half of the geoid at Tharsis might be explained by such a process. We note that the time necessary to form one or two plumes in these models is extraordinarily long, exceeding the age of the planet. Breuer *et al.* (1998) showed that that the exothermic olivine to β-spinel and β-spinel to γ-spinel phase transitions in the mantle tend to create a single stable area full of plumes, again a mechanism for Tharsis genesis. However, the model time necessary for this process to occur is about 1.5 Ga, far exceeding the bulk of Tharsis emplacement (Anderson *et al.*, 2001; Phillips *et al.*, 2001). Additionally, using a viscoelastic formulation for mantle flow, Zhong (2002) showed that plume structures likely account for less than 10% of the present geoid. Further, simultaneous consideration of both plume buoyancy and surface load to calculate the geoid-to-topography ratio indicates that a plume presently contributes less than 25% to the topography of Tharsis (Zhong and Roberts, 2003). Additional detailed analyses support the view that Tharsis is presently dominated by surface (and lithosphere) loading, as opposed to buoyant uplift from beneath the lithosphere (Lowry and Zhong, 2003; Roberts and Zhong, 2004). Redmond and King (2004) showed that it is possible in the present day for a plume model to contribute only very modestly to the Tharsis geoid and topography, while still producing a small amount of partial melt (as suggested by recent volcanism (Hartmann *et al.*, 1999)).

These results do not rule out the possibility that Tharsis had, at least in part, a plume origin (Spohn *et al.*, 2001). Most considerations are of a deep mantle plume (e.g., Schubert *et al.*, 1992), although Reese *et al.* (2004) suggest that the putative Tharsis plume could be thermochemical in origin, induced by an enormous impact. In support of a plume origin, we note that the Early–Middle Noachian circumferential graben in the Claritas Fossae region are consistent with buoyant uplift, not surface loading (Phillips *et al.*, 1990). However, buoyant uplift does not require a plume per se, and all models proposed thus far for Tharsis require such uplift because of the unavoidability of partial melting in the upper mantle and the intrusion of magmatic products in the crust (Finnerty *et al.*, 1988; Johnson and Phillips, 2005). Solomon and Head (1982) proposed that Tharsis formed over a region of warm mantle, resulting in substantial partial melting and a weak, thin lithosphere that focused the development of Tharsis. There are a number of possible mechanisms for creating a regionally warmer mantle. For example, Wenzel *et al.* (2004) show that the increased insulating effects of a thicker southern hemisphere crust (relative to a thinner northern one) (Neumann *et al.*, 2004) lead to long-lived upwellings beneath the southern highlands that may be a source for Tharsis volcanism. It is also possible, for a thin lithosphere, that the upper mantle was

heated by a flushing of the hot lower mantle via cold downwelling plumes from a convective upper boundary layer (van Thienen *et al*., 2006).

As we discuss below, models that treat Tharsis as a load on an elastic spherical shell have been very successful in predicting, quantitatively and spatially, the tectonic features associated with Tharsis. Further, there is a strong indication that this type of lithospheric loading has been operative since the end of the Noachian, and that by that time whatever dynamic process had been involved with the origin and early evolution of Tharsis had declined to a minor role. Thus we next discuss briefly the deformation styles on an elastic spherical shell.

5.2 Models for deformation on an elastic spherical shell

Mass loads on an elastic spherical shell will be supported by bending stresses, but more importantly by a resistance to changes in the radius of curvature of the shell if the horizontal scale of the load is of the order of or exceeds the planetary radius (Turcotte *et al*., 1981). Isostatic equilibrium will not equate to mass balance, even when bending stresses are negligible, because of partial to essentially full support of loads by membrane stresses.

Plate 19 shows an isostatic response function for Mars, and indicates that loads that are spatially represented by spherical harmonic degrees less than about eight are supported largely by membrane stresses. The load represented by the massive Tharsis rise falls into this category (in fact most of the power lies in $l = 2$ to 4), which indicates that the stress distribution is controlled by membrane forces.

Plate 20 illustrates the fundamental difference in stress distribution for bending and membrane stresses. For features small relative to planetary radius, a positive mass load at the surface creates an annular zone of radial extensional stress that would form circumferential normal faults. One-dimensionally, this is commonly observed on Earth at the flexural bulge that defines the subduction zone outer rise. On the Moon, this is manifested as circumferential graben surrounding impact basins with mass loads (mascons) (Solomon and Head, 1980; Golombek and McGill, 1983; Freed *et al*., 2001), and on Mars as circumferential graben surrounding large shield volcanoes, as well as the Isidis mascon basin (Comer *et al*., 1985). In contrast, when the diameter of the positive mass load approaches or exceeds the radius of the planet, the annular zone is subject to concentric extensional stresses, which can lead to radial normal faults (Banerdt *et al*., 1992), as observed emanating from the Tharsis region and discussed above.

The most rigorous model of deformation of a thin elastic spherical shell involves both vertical and horizontal loads (Vlasov, 1964) and has been adopted for planetary-scale geodynamical problems by Banerdt (1986). The horizontal load potential arises from horizontal gradients in lithostatic stress acting on vertical

planes, assuming uniaxial strain, as well as lithostatic stress acting on inclined horizontal planes. This term was missing from earlier thin-shell derivations (e.g., Turcotte *et al*., 1981), but incorporated in early thick-shell loading models (Phillips and Lambeck, 1980; Banerdt *et al*., 1982) for Tharsis. The solution of Banerdt (1986) is constrained to satisfy the geoid everywhere, and global surface and crust–mantle boundary topography (both referenced to the geoid) contribute to the load, in addition to net mass accommodated by deformation. Stress and strain are calculated from spherical coordinate system spatial gradients in deformation. A second approach modifies the model above by zeroing-out topography outside of Tharsis and proposes that the long-wavelength surface here is a deformed membrane (Phillips *et al*., 2001, 2004). The model has been successful in describing the shape of Mars, as described earlier, although the results are not necessarily unique. Finally, Dimitrova *et al*. (2006) approached this problem by solving the three-dimensional force balance equations for a thin lithosphere and crustal model constrained by the gravity field (Neumann *et al*., 2004) and topography, with the solution producing a global minimum in the second stress invariant.

5.3 Tharsis-induced stress and strain from elastic shell models

Previous lithospheric deformation models employing elastic-shell loading and based on Viking era gravity and topography (through degree and order eight), summarized in Banerdt *et al*. (1992), indicated that two different stress conditions were required to explain the tectonic features around Tharsis (Banerdt *et al*., 1982, 1992). Isostatic conditions lead to concentric extensional stresses on the topographic rise and radial compressional stresses around the edge that could account for the radial grabens on the rise and the concentric wrinkle ridges around the edge. A global compressive stress field may have modulated the formation of the concentric wrinkle ridges at the time when their formation peaked on Mars (Tanaka *et al*., 1991). However, the isostatic model could not explain all of the Tharsis-related tectonic features, as flexural (bending plus membrane) loading stresses were needed to develop the concentric extensional stresses needed to produce the radial grabens beyond the edge of the topographic rise.

Lithospheric deformation models based on the Mars Global Surveyor gravity and MOLA topography simplified the stress states required to explain most of the tectonic features around Tharsis (Banerdt and Golombek, 2000) (Plates 21 and 22). Flexural loading stresses based on present-day gravity and topography appear to explain successfully the location and orientation of most tectonic features. Specifically, the orientation of extensional grabens and rifts in Memnonia, Sirenum, Thaumasia, southern Claritas, Valles Marineris, Tempe and Mareotis Fossae are all accounted for by the flexural loading stresses, and the distribution agrees with

modeled areas with high strain. In addition, the orientation of compressional wrinkle ridges in Lunae, Solis, and Syria Plana, Sirenum, and Acidalia are explained by flexural loading stresses, and their distribution corresponds to highly strained areas in the model. Only extensional structures around Alba (which appears related to local volcanotectonic processes (Zuber *et al*., 2000; Cailleau *et al*., 2003, 2005)) and local structures around the Tharsis Montes and in Noctis Labyrinthus are not explained by the model. Early Noachian circumferential extensional structures in the Noctis Labyrinthus region (Phillips *et al*., 1990; Johnson and Phillips, 2005) can be explained with a thin elastic shell model and a net upward load (Banerdt *et al*., 1992).

In addition to explaining the orientation and distribution of most tectonic features around Tharsis, the extensional hoop strain predicted by the flexural loading model (0.2–0.4%) (Plate 21) agrees with the estimated extension and averaged strain across deformed regions around Tharsis. Estimates of extension across Tempe Terra (Golombek *et al*., 1996; Harrington *et al*., 1999; Hauber and Kronberg, 2001), Alba Patera (Plescia, 1991a) and Ceraunius Fossae (Borraccini *et al*., 2005), the central portion of Vallis Marineris (Schultz, 1995; Mege and Masson, 1996b), Sirenum and Thaumasia (Golombek *et al*., 1994, 1997; Hauber and Kronberg, 2005; Grott *et al*., 2007b) are reported in Table 5.2. Tempe, Alba, Sirenum and Thaumasia each occupy about an eighth section of Tharsis (roughly 2000 km across); Valles Marineris and Olympus, between Alba and Sirenum (which has negligible extension), each occupy a quarter section (roughly 4000 km across). As a result, extensional strain varies significantly from 0 to 1–2% across different 2000-km and 4000-km wide regions around Tharsis (Table 5.2), even though strain across individual structures with smaller widths can be as high as 5–20%. Taken together these estimates suggest a total circumferential extension of order $\sim$70 km, with an uncertainty of about $\pm$50 km (from possible variations in fault dip). For a 2500 km radius (or circumference of 15 700 km), these results suggest a total circumferential extensional strain of 0.4% $\pm$ 0.3% now expressed at the surface (not accounting for buried structures), which matches the model result. Estimates of the measurable shortening across wrinkle ridges in Lunae and Solis Plana and Arcadia Planitia radial to Tharsis suggest comparably low regional strains of 0.1–0.3% (Golombek *et al*., 1991, 2001; Plescia, 1991b, 1993). Concentric Late Noachian/Early Hesperian thrust structures south of Tharsis (Schultz and Tanaka, 1994) also suggest bulk shortening of 2–4 km and strain of 0.1–0.3% over radial transects of $\sim$1500 km in Sirenum. Both of these estimates of radial compressional strain agree with model results of 0.2–0.3% in Lunae and Solis Plana and 0.1–0.2% in Sirenum (Banerdt and Golombek, 2000) (Plate 22).

The observations that flexural (bending plus membrane) loading lithospheric stress models based on present-day gravity and topography can explain the observed

Table 5.2. *Hoop extension and strain around Tharsis*

Tharsis Province	Hoop extension ± uncertainty (km)*	Strain (%)**	Length (km)***
Alba	8 ± 5	0.4	2000
Ceraunius Fossae	40 ± 24	2	2000
Tempe Terra	20 ± 15	1	2000
Valles Marineris	20–30 ± 15–20	0.6	4000
Thaumasia (total)	18 ± 11	1	2000
Claritas Fossae	4 ± 2		
Thaumasia Fossae	11 ± 8	0.5	2000
Coracis Fossae	2 ± 1		
Sirenum	3 ± 2	0.1	2000
Olympus	0	0	4000

*Extension concentric to the center of Tharsis at a radial distance of ∼2500 km as estimated from references in the text. The quoted formal uncertainty is from the possible variations in fault dip (Golombek *et al*., 1996). Strain **estimated from the extension over length ***of pie-shaped sector that province occupies.

distribution and strain of radial and compressional structures, coupled with the mapping results that suggest over half of the radial structures formed by the Middle Noachian, argue strongly that the basic lithospheric structure of the province has changed little since the Middle Noachian. The lithospheric deformation models require the load to be huge (of the scale of Tharsis, large relative to the radius of the planet), and the mapping requires the load that caused the flexure to have been in place by the Middle Noachian (>3.8 Ga). Subsequent deformation events around Tharsis appear consistent with the same overall lithospheric structure, with relatively minor changes in the centers of deformation (e.g., Anderson *et al*., 2001). Fine layers within Valles Marineris revealed by the Mars Orbiter Camera have been interpreted as being lava flows that are Late Noachian or older (McEwen *et al*., 1999). These volcanics are therefore likely part of the load that caused the flexure around Tharsis.

The emplacement of the Tharsis load ($\sim 3 \times 10^8$ km^3) (Phillips *et al*., 2001) may have contributed to wetter and likely warmer periods during the Noachian. If the load is composed largely of volcanics, as suggested by fine layers within Valles Marineris (McEwen *et al*., 1999), water released with the magma would be equivalent to a global layer up to 100 m thick, which could have had a significant impact on the Martian climate (Phillips *et al*., 2001). Impact processes may have also contributed to short-lived clement environments (e.g., Segura *et al*., 2002).

6 Models and tectonic comparisons: other global-scale features

6.1 Models for global isotropic stress and strain

Investigations on other terrestrial planets show that regional to global tectonics can be the result of the superposition of stresses from regional loads and stresses from global contraction of the cooling planet. On Venus, regional control of otherwise isotropic compressional strain appears to have oriented ridges surrounding Aphrodite Terra (Sandwell *et al*., 1997), and global contraction has been suggested to modulate the formation of wrinkle ridges in and around mascon basins on the Moon (Solomon and Head, 1980). Mercury has long been recognized for its surface manifestation (thrust faults) of global contraction, presumably due to cooling (Watters and Nimmo, 2009), and imaging from the MESSENGER spacecraft has increased (and will continue to increase as more data are acquired) the estimated magnitude of the areal density of thrust faults and thus estimates of total contractional strain (Solomon *et al*., 2008).

Mars appears to be no different than these other planets. Pervasive wrinkle ridge occurrence on volcanic plains of Early Hesperian age strongly suggests a global contractional event of Early to Late Hesperian. Stresses from Tharsis have global influences (Phillips *et al*., 2001) and this is an obvious source of deformation. Furthermore, most of the wrinkle ridges in the western hemisphere (including those in northern plains (Head *et al*., 2002)) are circumferential to Tharsis, implying a causal relationship (Wise *et al*., 1979; Watters, 1993; Anderson *et al*., 2001). Tharsis-circumferential wrinkle ridges are also present in the northern lowlands of the eastern hemisphere (Head *et al*., 2002). However, significant populations of wrinkle ridges are also found in the eastern hemisphere (e.g., Hesperia and Syrtis Major Plana) and northern basins (e.g., Utopia and Isidis) that have little obvious relationship with Tharsis, and yet most wrinkle ridges appear to have formed in the time period spanning the Early Hesperian to the Early Amazonian (Tanaka *et al*., 1991, 2003, 2005; Mangold *et al*., 2000). These globally-pervasive wrinkle ridges may have resulted from a globally isotropic contractional strain event during this time interval that was modulated by Tharsis stresses in the western hemisphere and northern plains, and by Tharsis and other loads, such as Utopia in the eastern hemisphere. It is possible that due to growing global contractional stresses, the onset of pervasive wrinkle-ridge formation marks a reorientation of principal stresses to form thrust faults rather than extensional or strike-slip faults induced by Tharsis and other loads (e.g., Okubo and Schultz, 2006; Andrews-Hanna *et al*., 2008b).

Secular cooling is the obvious mechanism for producing isotropic global contraction on Mars (Schubert *et al*., 1992; Mangold *et al*., 2000). Modeling by Andrews-Hanna *et al*. (2008b) has shown that the isotropic compressive stresses required to explain the transition from strike-slip faulting to thrust faulting in

circum-Tharsis regions produces the observed amount of compressional strain of about 0.1% (e.g., Golombek *et al*., 1991, 2001). They show that such strain magnitudes also result from contractional strain produced by thermal models, with the addition of loading effects from Tharsis.

6.2 Models for origin of the global dichotomy

The origin of the planetary dichotomy that separates the smooth northern lowlands from the heavily cratered southern highlands has remained an enigma since first discussed over thirty years ago (Hartmann, 1973). Hypotheses for its genesis can be broadly divided into endogenic and exogenic. Exogenic theories have it that one (Wilhems and Squyres, 1984) or more (Frey and Schultz, 1988) large impacts were responsible for the lowering of the crustal surface in the northern hemisphere. Endogenic theories involve several types of processes for thinning the crust dynamically from within (e.g., Wise *et al*., 1979), and include the possibility of plate tectonics (Sleep, 1994). In the last five years, improved sophistication in dynamic modeling, as well as new data from missions, have provided fresh constraints on the origin of the dichotomy.

The most important findings bearing on the origin of the dichotomy come from MGS data: (1) The underlying crust of the northern lowlands is nearly as old (or as old, given uncertainties) as the crust of the southern highlands (Frey *et al*., 2002; Frey, 2006a,b), implying that their crustal ages are essentially the same. (2) The northern and southern crusts have distinctive thicknesses (Zuber *et al*., 2000; Zuber, 2001; Neumann *et al*., 2004, 2008). (3) As mentioned earlier, the northern lowlands crust contains widespread but modest magnetic anomalies (Mitchell *et al*., 2007). This implies that this crust formed, (a) during the waning stages of the dynamo, (b) lacked large igneous intrusions to acquire stronger remanent magnetization, or (c) was affected by demagnetization processes associated with water. Regarding (c), it is possible that magnetization in the northern lowlands is more robust than observed, but the dominant wavelengths of the anomalies are below the resolution of the MGS magnetic field or electron reflectometry data sets. Selective removal of magnetic anomalies by hydrothermal alteration has been proposed as a means of shifting the power in the magnetic field spectrum to shorter wavelengths (Solomon *et al*., 2005).

If the northern crust is pre-Noachian (Nimmo and Tanaka, 2005; Frey, 2006a), then it could be a feature of primary crustal fractionation, possibly associated with core formation, which took place immediately after planetary accretion (Lee and Halliday, 1997). Variations in crustal thickness associated with the Utopia basin in the northern lowlands are mostly preserved, suggesting that any crustal thinning must have occurred before the basin-forming impact (Neumann *et al*., 2004, 2008).

As noted above, a very early origin for the crustal dichotomy raises the question as to why there are so few magnetic anomalies in the northern lowlands, and challenges the primary crustal fractionation hypothesis. A multiple-impact origin (Frey and Schultz, 1988) for the crustal dichotomy requires an unlikely preferential bombardment in what is now the northern hemisphere. Multiple impacts also provide no simple way to remove ejecta from the northern hemisphere (McGill and Squyres, 1991), and thus it is difficult to see how multiple, large impacts could strip the northern hemisphere crust nearly uniformly (Zuber *et al*., 2000; Zuber, 2001; Neumann *et al*., 2004) to a depth of ∼3 km.

As discussed earlier, the arguments for a single impact origin for the northern lowlands (Wilhems and Squyres, 1984) have been considerably strengthened by the work of Andrews-Hanna *et al*. (2008a) on the shape of the northern lowlands and by Marinova *et al*. (2008) on numerical modeling of a single impact. Nimmo *et al*. (2008) have provided a potential constraint on the timing of the mega-impact in that their numerical simulations show that the lowlands crust is likely derived from a deep, depleted mantle source, which may be akin to shergottite meteorites, which likely formed ∼100 Myr after planet formation. In this scenario, the dynamo was waning by this time in order to produce weaker anomalies in the lowlands crust. Overall, the impact hypothesis for the origin of the crustal dichotomy appears to suffer fewer problems than others that have been proposed. It occurs very early in Mars' history, provides a ready explanation for the elliptical shape of the lowlands and thinned crust, and fits in conceptually with large impacts having an important role in the early formation and evolution of the terrestrial planets (aka the giant impact hypothesis for the origin of the Earth's moon).

The relation of the formation of the northern lowlands to the formation of Tharsis is another issue that has been considered qualitatively (Wise *et al*., 1979) and quantitatively (Wenzel *et al*., 2004). Endogenic theories for the formation of the crustal dichotomy, whether Tharsis is involved or not, are usually concerned with the generation of spherical harmonic degree $l = 1$ mantle convection (i.e., single regions of upgoing and downgoing flow). Zhong and Zuber (2001) showed that degree-1 mantle convection is possible in Mars with a central core if the upper mantle viscosity is ∼100 times smaller than that of the lower mantle. The onset of degree-1 mantle convection is delayed in their model runs, which may be in conflict with the pre-Noachian age of both the northern and southern crusts; more recent work with degree-1 convection in layered viscosity models shows that timescales as short as 100 Myr can be achieved (Roberts and Zhong, 2006).

The idea that the northern hemisphere crust is a relic "oceanic" plate from a plate tectonics era was advanced by Sleep (1994), based mainly on the low elevation and presumed (at the time of publication) thinner crust in the north. Subsequently, the thinner (and approximately constant thickness) crust was confirmed (Zuber

et al., 2000). Under this hypothesis, the dichotomy boundary is made up of the three classic types of oceanic plate margins. However, geological predictions of this model appear to fail (Pruis and Tanaka, 1995; Sleep and Tanaka, 1995). Further, the recognition that the northern highlands crust is pre-Noachian in age (Frey *et al*., 2002; Frey, 2006a) with younger circular basins (QCDs and Utopia) unaffected by plate tectonic processes pushes the episode to very early in Martian history, and thus this hypothesis is difficult to test. It may be worth noting that the areal growth of the southern highlands crust might have shut down a very early (no longer recognizable) episode of plate tectonics when the fractional planetary coverage exceeded 50% (Lenardic *et al*., 2004), a scenario seemingly at odds with a primordial origin for the crustal dichotomy.

The dichotomy boundary separates the two distinct crustal provinces of Mars, except in northwestern Arabia Terra where low-standing highlands terrain appears to belong to the northern province (Zuber *et al*., 2000), or is a transitional form between the two provinces (Zuber, 2001; Neumann *et al*., 2004, 2008), and where Tharsis volcanics have obscured the boundary. Subsequent erosional processes and possible deformation in the Late Noachian/Early Hesperian (McGill and Dimitriou, 1990; Smrekar *et al*., 2004) suggest ongoing activity at the dichotomy boundary. Once the basic elevation difference of the crustal provinces was created, processes could have operated subsequently to create a sharp boundary in places (Guest and Smrekar, 2005). Mechanisms proposed include faulting in response to flexural stresses caused by the differences in crustal thickness and the resulting broad-scale topography (Watters, 2003a,b), and faulting due to relaxation of the dichotomy boundary by lower crustal flow (Guest and Smrekar, 2005). As noted above, mass wasting and fluvial erosion could have modified the steep gradients caused by faulting, as well as the crustal stress fields.

7 Concluding remarks

Our knowledge of Mars tectonics has improved dramatically since publication of the last major review based on Viking data (Banerdt *et al*., 1992). Mars Global Surveyor has provided our first high-definition view of the global topography, geoid and gravity fields, which have allowed definition of global crustal thickness and substantially improved modeling of global and regional geodynamical and geological processes. In addition, geologic mapping of tectonized regions has defined the major phases of deformation within the global stratigraphic framework (Tanaka, 1986), and investigations of the geometry and kinematics of observed structures have yielded broad estimates of shortening and extension across these regions. As a result, higher fidelity geodynamical models can be constructed and then tested and constrained much better than was possible before.

This work shows that some process or processes in the pre-Noachian thinned the crust and lowered the surface by several kilometers in the northern hemisphere of Mars. This thinning could have been the result of primordial crustal fractionation, degree-1 convection processes, or a single mega-impact. The latter hypothesis has been considerably strengthened by the recognition that the shape of the northern lowlands with Tharsis removed match a large elliptical basin consistent with a large oblique impact early in Mars' history. Subsequently, these northern lowlands (roughly a third of the planet) were resurfaced (thinly, 1–2 km) over a period of time extending into the Hesperian (and, modestly, into the Amazonian).

The global shape of Mars (outside of the spin oblateness) is dominated by the pole-to-pole slope and the enormous Tharsis rise (load) and the global deformation it produced (surrounding flexural moat and antipodal bulge). Lithospheric membrane/flexural loading models based on present-day global gravity and topography appear capable of explaining the orientation, distribution and strain found in the giant radiating extensional grabens and concentric compressional ridges that cover the entire western hemisphere and northern plains.

Geologic mapping shows that deformation (radiating grabens) around Tharsis peaked in the Noachian and decreased with relatively minor changes in centers of deformation through time, arguing that the basic lithospheric structure of Mars has changed little since the Middle Noachian. Structures exposed in the eastern hemisphere record local loading around basins (including those in the northern plains) and volcanoes, compressional lobate ridges and extensional faults associated with the dichotomy boundary, and far-field effects of Tharsis. Wrinkle ridge formation in volcanic provinces of the eastern hemisphere, in the northern plains, and around Tharsis appears to have peaked globally in the Hesperian, likely modulated by global contraction.

The outpouring of volcanics responsible for the development and growth of Tharsis appear capable of producing the likely early warmer and wetter conditions that formed the valley networks, dry lake beds, and high erosion rates preserved in degraded craters and terrain, the exposures of Noachian phyllosilicates mapped by OMEGA and CRISM, and the wet conditions indicated by the Meridiani Planum sulfate evaporites and aqueous altered rocks of the Columbia Hills discovered by the Mars Exploration Rovers.

Acknowledgments

MPG was supported by grants from the Planetary Geology and Geophysics Program of the National Aeronautics and Space Administration at the Jet Propulsion Laboratory, California Institute of Technology, under a contract with NASA. RJP

was supported by NASA grants from the Mars Data Analysis and Planetary Geology and Geophysics Programs. The authors appreciate constructive comments from K. Tanaka, P. McGovern and G. McGill and Figures from Steven A. Hauck II (Plate 13), Kris Larsen (Plates 17 and 18) and Bruce Banerdt (Plates 21 and 22).

References

Acuña, M. H., Connerney, J. E. P., Ness, N. F., Lin, R. P., Mitchell, D., Carlson, C. W., McFadden, J., Anderson, K. A., Rème, H., Mazelle, C., Vignes, D., Wasilewski, P., and Cloutier, P. (1999). Global distribution of crustal magnetization discovered by the Mars Global Surveyor MAG/ER experiment. *Science*, **284**, 790–793.

Allemand, P. and Thomas, P. G. (1995). Localization of Martian ridges by impact craters: Mechanical and chronological implications. *J. Geophys. Res.*, **100**, 3251–3262.

Anderson, S. and Grimm, R. E. (1998). Rift processes at the Valles Marineris, Mars: Constraints from gravity on necking and rate-dependent strength evolution. *J. Geophys. Res.*, **103**, 11 113–11 124.

Anderson, R. C., Dohm, J. M., Golombek, M. P., Haldemann, A. F. C., Franklin, B. J., Tanaka, K. L., Lias, J., and Peer, B. (2001). Primary centers and secondary concentrations of tectonic activity through time in the western hemisphere of Mars. *J. Geophys. Res.*, **106**, 20 563–20 585.

Anderson, R. C., Dohm, J. M., Haldemann, A. F. C., Hare, T. M., and Baker, V. R. (2004). Tectonic histories between Alba Patera and Syria Planum, Mars. *Icarus*, **171**, 31–38.

Anderson, R. C., Dohm, J. M., Haldemann, A. F. C., Pounders, E., Golombek, M., and Castano, A. (2008). Centers of tectonic activity in the eastern hemisphere of Mars. *Icarus*, **195**, 537–546.

Andrews-Hanna, J. C., Phillips, R. J., and Zuber, M. T. (2007). Meridiani Planum and the global hydrology of Mars. *Nature*, **446**, 163–166.

Andrews-Hanna, J. C., Zuber, M. T., and Banerdt, W. B. (2008a). The Borealis basin and the origin of the Martian crustal dichotomy. *Nature*, **453**, 1212–1215.

Andrews-Hanna, J. C., Zuber, M. T., and Hauck I, S. A. (2008b). Strike-slip faults on Mars: Observations and implications for global tectonics and geodynamics. *J. Geophys. Res.*, **113**, doi:10.1029/2007JE002980.

Anguita, F., Farelo, A. F., Lopez, V., Mas, C., Munoz-Espadas, M. J., Marquez, A., and Ruiz, J. (2001). Tharsis dome, Mars: New evidence for Noachian-Hesperian thick-skin and Amazonian thin-skin tectonics. *J. Geophys. Res.*, **106**, 7577–7589.

Anguita, F., Fernández, C., Cordero, G., Carrasquilla, S., Anguita, J., Núñez, A., Rodríguez, S., and García, J. (2006). Evidences for a Noachian–Hesperian orogeny in Mars. *Icarus*, **185**, 331–357.

Arkani-Hamed, J. (2001). A 50-degree spherical harmonic model of the magnetic field of Mars. *J. Geophys. Res.*, **106**, 23 197–23 208.

Arkani-Hamed, J. and Boutin, D. (2004). Paleomagnetic poles of Mars: Revisited. *J. Geophys. Res.*, **109**, doi:10.1029/2003JE002229; see also correction doi:10.1029/2004JE002278.

Arvidson, R., Guiness, E., and Lee, S. (1979). Differential aeolian redistribution rates on Mars. *Nature*, **278**, 533–535.

Baker, V. R., Carr, M. H., Gulick, V. C., Willemann, C. R., and Marley, M. S. (1992). Channels and valley networks. In *Mars*, ed. H. H. Kieffer, B. M. Jakosky, C. W. Snyder and M. S. Matthews. Tucson, AZ: University of Arizona Press, pp. 493–522.

Banerdt, W. B. (1986). Support of long-wavelength loads on Venus and implications for internal structure. *J. Geophys. Res.*, **91**, 403–419.
Banerdt, W. B. and Golombek, M. P. (2000). Tectonics of the Tharsis region of Mars: Insights from MGS topography and gravity (abs.). *Lunar Planet. Sci. Conf. XXXI*, 2038. Houston, TX: Lunar and Planetary Institute (CD-ROM).
Banerdt, W. B., Phillips, R. J., Sleep, N. H., and Saunders, R. S. (1982). Thick shell tectonics on one-plate planets: Applications to Mars. *J. Geophys. Res.*, **87**, 9723–9733.
Banerdt, W. B., Golombek, M. P., and Tanaka, K. L. (1992). Stress and tectonics on Mars. In *Mars*, ed. H. H. Kieffer, B. M. Jakosky, C. W. Snyder and M. S. Matthews. Tucson, AZ: University of Arizona Press, pp. 249–297.
Belleguic, V., Lognonné, P., and Wieczorek, M. (2005). Constraints on the Martian lithosphere from gravity and topography data. *J. Geophys. Res.*, **110**, doi:10.1029/2005JE002437.
Bibring, J.-P., Langevin, Y., Mustard, J., Poulet, F., Arvidson, R., Gendrin, A., Gondet, B., Mangold, N., Pinet, P., Forget, F., and the-Omega-team (2006). Global mineralogical and aqueous Mars history derived from OMEGA/Mars Express data. *Science*, **312**, 400–404.
Biswas, S. and Ravat, D. (2005). Why meaningful paleopoles can't be determined without special assumptions from Mars Global Surveyor data? (abs.) *Lunar Planet. Sci. Conf. XXXVI*, 2192. Houston, TX: Lunar and Planetary Institute (CD-ROM).
Borgia, A., Burr, J., Montero, W., Morales, L. D., and Alvarado, G. E. (1990). Fault propagation folds induced by gravitational failure and slumping of the volcanic edifices. *J. Geophys. Res.*, **95**, 14 357–14 382.
Borraccini, F., Lanci, L., Wezel, F. C., and Baioni, D. (2005). Crustal extension in the Ceraunius Fossae, Northern Tharsis Region, Mars. *J. Geophys. Res.*, **110**, doi:10.1029/2004JE002373.
Borraccini, F., Lanci, L., and Wezel, F. C. (2006). Does a detachment level exist beneath the Ceraunius Fossae? Insights from graben mapping and lost-area balancing analysis. *Planet. Space Sci.*, **54**, 701–709.
Borraccini, F., Di Achille, G., Ori, G. G., and Wezel, F. C. (2007). Tectonic evolution of the eastern margin of the Thaumasia Plateau (Mars) as inferred from detailed structural mapping and analysis. *J. Geophys. Res.*, **112**, doi:10.1029/2006JE002866.
Brace, W. F. and Kohlstedt, D. L. (1980). Limits on lithospheric stress imposed by laboratory experiments. *J. Geophys. Res.*, **85**, 6248–6252.
Breuer, D., Yuen, D. A., Spohn, T., and Zhang, S. (1998). Three dimensional models of Martian mantle convection with phase transitions. *Geophys. Res. Lett.*, **25**, 229–232.
Burr, D. M., Grier, J. A., Keszthelyi, L. P., and McEwen, A. S. (2002a). Repeated aqueous flooding from the Cerberus Fossae: Evidence for very recently extant, deep groundwater on Mars. *Icarus*, **159**, 53–73.
Burr, D. M., McEwen, A. S., and Sakimoto, S. E. H. (2002b). Recent aqueous floods from the Cerberus Fossae. *Geophys. Res. Lett.*, **29**, doi:10.1029/2001GL013345.
Cailleau, B., Walter, T. R., Janle, P., and Hauber, E. (2003). Modeling volcanic deformation in a regional stress field: Implications for the formation of graben structures on Alba Patera, Mars. *J. Geophys. Res.*, **108**, doi:10.1029/2003JE002135.
Cailleau, B., Walter, T. R., Janle, P., and Hauber, E. (2005). Unveiling the origin of radial grabens on Alba Patera volcano by finite element modeling. *Icarus*, **176**, 44–56.
Carr, M. H. (1996). *Water on Mars*. New York: Oxford University Press.
Chicarro, A., Schultz, P. H., and Masson, P. (1985). Global and regional ridge patterns on Mars. *Icarus*, **63**, 153–174.

Comer, R. P., Solomon, S. C., and Head, J. W. (1985). Mars: Thickness of the lithosphere from the tectonic response to volcanic loads. *Rev. Geophys.*, **23**, 61–92.
Connerney, J. E. P., Acuña, M. H., Wasilewski, P., Ness, N. F., Rème, H., Mazelle, C., Vignes, D., Lin, R. P., Mitchell, D., and Cloutier, P. (1999). Magnetic lineations in the ancient crust of Mars. *Science*, **284**, 794–798.
Courtillot, V. E., Allegre, C. J., and Mattauer, M. (1975). On the existence of lateral relative motions on Mars. *Earth Planet. Sci. Lett.*, **25**, 279–285.
Craddock, R. A. and Howard, A. D. (2002). The case for rainfall on a warm, wet early Mars. *J. Geophys. Res.*, **107**, doi:5110.1029/2001JE001505.
Crumpler, L. S. and Aubele, J. C. (1978). Structural evolution of Arsia Mons, Pavonis Mons, and Ascreus Mons: Tharsis region of Mars. *Icarus*, **34**, 496–541.
Crumpler, L. S., Head, J. W., and Aubele, J. C. (1996). Calderas on Mars: Characteristics, structure, and associated flank deformation. In *Volcano Instability on the Earth and Other Planets. Geol. Soc. Am. Spec. Publ. No. 110*, ed. W. J. Mcguire, A. P. Jones and J. Neuberg, pp. 307–348.
Davis, P. A. and Golombek, M. P. (1990). Discontinuities in the shallow Martian crust at Lunae, Syria, and Sinai Plana. *J. Geophys. Res.*, **95**, 14 231–14 248.
Davis, P. A., Tanaka, K. L., and Golombek, M. P. (1995). Topography of closed depressions, scarps, and grabens in the north Tharsis region of Mars: Implications for shallow crustal discontinuities and graben formation. *Icarus*, **114**, 403–422.
Dimitrova, L. L., Holt, W. E., Haines, A. J., and Schultz, R. A. (2006). Toward understanding the history and mechanisms of Martian faulting: The contribution of gravitational potential energy. *Geophys. Res. Lett.*, **33**, L08202, doi:10.1029/2005GL025307.
Dohm, J. M. and Tanaka, K. L. (1999). Geology of the Thaumasia region, Mars: Plateau development, valley origins, and magmatic evolution. *Planet. Space Sci.*, **47**, 411–431.
Dohm, J. M., Tanaka, K. L., and Hare, T. M. (2001). Geologic, paleotectonic, and paleoerosional maps of the Thaumasia Region, Mars. U.S. Geol. Surv. Geol. Invest. Ser., Map I-2650.
Ernst, R. E., Grosfils, E. B., and Mege, D. (2001). Giant dike swarms: Earth, Venus and Mars. *Annu. Rev. Earth Planet. Sci.*, **29**, 489–534.
Erslev, E. A. (1991). Trishear fault-propagation folding. *Geology*, **19**, 617–620.
Fernández, C. and Anguita, F. (2007). Oblique rifting at Tempe Fossae, Mars. *J. Geophys. Res.*, **112**, doi:10.1029/2007JE002889.
Ferrill, D. A., Wyrick, D. Y., Morris, A. P., Sims, D. W., and Franklin, N. M. (2004). Dilational fault slip and pit chain formation on Mars. *GSA Today*, **14**, 4–12.
Finnerty, A. A., Phillips, R. J., and Banerdt, W. B. (1988). Igneous processes and the closed system evolution of the Tharsis region of Mars. *J. Geophys. Res.*, **93**, 10 225–10 235.
Folkner, W. M., Yoder, C. F., Yuan, D. N., Standish, E. M., and Preston, R. A. (1997). Interior structure and seasonal mass redistribution of Mars from radio tracking of Mars Pathfinder. *Science*, **278**, 1749–1752.
Forsythe, R. D. and Zimbelman, J. R. (1988). Is the Gordii Dorsum escarpment on Mars an exhumed transcurrent fault? *Nature*, **336**, 143–146.
Francis, P. W. and Wadge, G. (1983). The Olympus Mons aureole: Formation by gravitational spreading. *J. Geophys. Res.*, **88**, 8333–8344.
Freed, A. M., Melosh, H. J., and Solomon, S. C. (2001). Tectonics of mascon loading: Resolution of the strike-slip faulting paradox. *J. Geophys. Res.*, **106**, 20 603–20 620.

Frey, H. (1979). Martian canyons and African rifts: Structural comparisons and implications. *Icarus*, **37**, 142–155.
Frey, H. V. (2006a). Impact constraints on the age and origin of the lowlands of Mars. *Geophys. Res. Lett.*, **33**, doi:10.1029/2005GL024484.
Frey, H. V. (2006b). Impact constraints on, and a chronology for, major events in early Mars history. *J. Geophys. Res.*, **111**, doi:10.1029/2005JE002449.
Frey, H. V. and Schultz, R. A. (1988). Large impact basins and the mega-impact origin for the crustal dichotomy on Mars. *Geophys. Res. Lett.*, **15**, 229–232.
Frey, H., Sakimoto, S. E., and Roark, J. (1998). The MOLA topographic signature at the crustal dichotomy boundary zone on Mars. *Geophys. Res. Lett.*, **25**, 4409–4412.
Frey, H. V., Roark, J. H., Shockey, K. M., Frey, E. L., and Sakimoto, S. E. H. (2002). Ancient lowlands on Mars. *Geophys. Res. Lett.*, **29**, doi:10.1029/2001GL013832.
Golombek, M. P. (1985). Fault type predictions from stress distributions on planetary surfaces: Importance of fault initiation depth. *J. Geophys. Res.*, **90**, 3065–3074.
Golombek, M. P. (2003). The surface of Mars: Not just dust and rocks. *Science*, **300**, 2043–2044.
Golombek, M. P. and Bridges, N. T. (2000). Erosion rates on Mars and implications for climate change: Constraints from the Pathfinder landing site. *J. Geophys. Res.*, **105**, 1841–1853.
Golombek, M. P. and McGill, G. E. (1983). Grabens, basin tectonics, and the maximum total expansion of the Moon. *J. Geophys. Res.*, **88**, 3563–3578.
Golombek, M. P., Plescia, J. B., and Franklin, B. J. (1991). Faulting and folding in the formation of planetary wrinkle ridges. *Proc. Lunar Planet. Sci. Conf. 21*, 679–693.
Golombek, M. P., Tanaka, K. L., Chadwick, D. J., Franklin, B. J., and Davis, P. A. (1994). Extension across Tempe Terra and Sirenum provinces on Mars from measurements of fault scarp widths (abs.). *Lunar Planet. Sci. Conf. XXV*. Houston, TX: Lunar and Planetary Institute, 443–444.
Golombek, M. P., Tanaka, K. L., and Franklin, B. J. (1996). Extension across Tempe Terra, Mars, from measurements of fault scarp widths and deformed craters. *J. Geophys. Res.*, **101**, 26 119–26 130.
Golombek, M. P., Franklin, B. J., Tanaka, K. L., and Dohm, J. M. (1997). Extension through time across Thaumasia (abs.). *Lunar Planet. Sci. Conf. XXVIII*. Houston, TX: Lunar and Planetary Institute, 431–432.
Golombek, M. P., Anderson, F. S., and Zuber, M. T. (2001). Martian wrinkle ridge topography: Evidence for subsurface faults from MOLA. *J. Geophys. Res.*, **106**, 23 811–23 821.
Golombek, M. P., Crumpler, L. S., Grant, J. A., Greeley, R., Cabrol, N. A., Parker, T. J., Rice Jr., J. W., Ward, J. G., Arvidson, R. E., Moersch, J. E., Fergason, R. L., Christensen, P. R., Castaño, A., Castaño, R., Haldemann, A. F. C., Li, R., Bell III, J. F., and Squyres, S. W. (2006a). Geology of the Gusev cratered plains from the Spirit rover transverse. *J. Geophys. Res.*, **111**, doi:10.1029/2005JE002503.
Golombek, M. P., Grant, J. A., Crumpler, L. S., Greeley, R., Arvidson, R. E., Bell III, J. F., Weitz, C. M., Sullivan, R., Christensen, P. R., Soderblom, L. A., and Squyres, S. W. (2006b). Erosion rates at the Mars Exploration Rover landing sites and long-term climate change on Mars. *J. Geophys. Res.*, **111**, doi:10.1029/2006JE002754.
Goudy, C. L. and Schultz, R. A. (2005). Dike intrusions beneath grabens south of Arsia Mons, Mars. *Geophys. Res. Lett.*, **32**, doi:10.1029/2004GL021977.
Grant, J. A., Arvidson, R., Bell III, J. F., Cabrol, N. A., Carr, M. H., Christensen, P., Crumpler, L. S., Des Marais, D. J., Ehlmann, B. L., Farmer, J., Golombek, M., Grant, F. D., Greeley, R., Herkenhoff, K., Li, R., McSween, H. Y., Ming, D. W., Moersch, J.,

Rice Jr., J. W., Ruff, S., Richter, L., Squyres, S., Sullivan, R., and Weitz, C. (2004). Surficial deposits at Gusev crater along Spirit rover traverses. *Science*, **305**, 807–810.

Grimm, R. E. and Solomon, S. C. (1986). Tectonic tests of proposed polar wander paths for Mars and the Moon. *Icarus*, **65**, 110–121.

Grott, M. and Breuer, D. (2008). The evolution of the Martian elastic lithosphere and implications for crustal and mantle rheology. *Icarus*, **193**, 503–515.

Grott, M., Hauber, E., Werner, S. C., Kronberg, P., and Neukum, G. (2005). High heat flux on ancient Mars: Evidence from rift flank uplift at Coracis Fossae. *Geophys. Res. Lett.*, **32**, doi:10.1029/2005GL023894.

Grott, M., Hauber, E., Werner, S. C., Kronberg, P., and Neukum, G. (2007a). Mechanical modeling of thrust faults in the Thaumasia region, Mars, and implications for the Noachian heat flux. *Icarus*, **186**, 517–526.

Grott, M., Kronberg, P., Hauber, E., and Cailleau, B. (2007b). Formation of the double rift system in the Thaumasia Highlands, Mars. *J. Geophys. Res.*, **112**, doi:10.1029/2006JE002800.

Guest, A. and Smrekar, S. E. (2005). Relaxation of the Martian dichotomy boundary: Faulting in the Ismenius Region and constraints on the early evolution of Mars. *J. Geophys. Res.*, **110**, E12S25, doi:10.1029/2005JE002504.

Hall, J. L., Solomon, S. C., and Head, J. W. (1986). Elysium Region, and Mars: Tests of lithospheric loading models for the formation of tectonic features. *J. Geophys. Res.*, **91**, 11 377–11 392.

Hanna, J. C. and Phillips, R. J. (2006). Tectonic pressurization of aquifers in the formation of Mangala and Athabasca Valles, Mars. *J. Geophys. Res.*, **111**, doi:10.1029/2005JE002546.

Harder, H. (1998). Phase transitions and the three-dimensional planform of thermal convection in the Martian mantle. *J. Geophys. Res.*, **103**, 16 775–16 797.

Harder, H. (2000). Mantle convection and the dynamic geoid of Mars. *Geophys. Res. Lett.*, **27**, 301–304.

Harder, H. and Christensen, U. (1996). A one-plume model of Martian mantle convection. *Nature*, **380**, 507–509.

Harrington, B. W., Phillips, R. J., and Golombek, M. P. (1999). Extension across Tempe Terra, Mars from MOLA topographic measurements (abs.). *The Fifth International Conference on Mars*, 6130. Houston, TX: Lunar and Planetary Institute (CD-ROM).

Harris, S. A. (1977). The aureole of Olympus Mons. *J. Geophys. Res.*, **82**, 3099–3107.

Hartmann, W. K. (1973). Martian surface and crust: Review and synthesis. *Icarus*, **19**, 550–575.

Hartmann, W. K. (2005). Martian cratering 8: Isochron refinement and the chronology of Mars. *Icarus*, **174**, 294–320, doi:10.1016/j.icarus.2004.11.023.

Hartmann, W. K. and Neukum, G. (2001). Cratering chronology and evolution of Mars. *Space Sci. Rev.*, **96**, 165–194.

Hartmann, W. K., Malin, M. C., McEwen, A. S., Carr, M. H., Soderblom, L., Thomas, P., Danielson, E., James, P., and Veverka, J. (1999). Evidence for recent volcanism on Mars from crater counts. *Nature*, **397**, 586–589.

Hauber, E. and Kronberg, P. (2001). Tempe Fossae, Mars: A Planetary analog to a terrestrial continental rift? *J. Geophys. Res.*, **106**, 20 587–20 602.

Hauber, E. and Kronberg, P. (2005). The large Thaumasia graben on Mars: Is it a rift? *J. Geophys. Res.*, **110**, doi:10.1029/2005JE002407.

Hauck II, S. A. and Phillips, R. J. (2002). Thermal and crustal evolution of Mars. *J. Geophys. Res.*, **107**, doi:10.1029/2001JE001801.

Head, J. W., Kreslavsky, M. A., and Pratt, S. (2002). Northern lowlands of Mars: Evidence for widespread volcanic flooding and tectonic deformation in the Hesperian period. *J. Geophys. Res.*, **107**, doi:10.1029/2000JE001445.

Hiesinger, H. and Head, J. W. (2004). The Syrtis Major volcanic province, Mars: Synthesis from Mars Global Surveyor data. *J. Geophys. Res.*, **109**, doi:10.1029/2003JE002143.

Hood, L. L., Young, C. N., Richmond, N. C., and Harrison, K. P. (2005). Modeling of major Martian magnetic anomalies: Further evidence for polar reorientations during the Noachian. *Icarus*, **177**, 144–173.

Howard, A. D., Moore, J. M., and Irwin III, R. P. (2005). An intense terminal epoch of widespread fluvial activity on early Mars: 1. Valley network incision and associated deposits. *J. Geophys. Res.*, **110**, doi:10.1029/2005JE002459.

Irwin III, R. P., Howard, A. D., Craddock, R. A., and Moore, J. M. (2005). An intense terminal epoch of widespread fluvial activity on early Mars: 2. Increased runoff and paleolake development. *J. Geophys. Res.*, **110**, doi:10.1029/2005JE002460.

Ivanov, M. A. and Head, J. W. (2006). Alba Patera, Mars: Topography, structure, and evolution of a unique late Hesperian – early Amazonian shield volcano. *J. Geophys. Res.*, **111**, doi:10.1029/2005JE002469.

Jaeger, W. L., Keszthelyi, L. P., Mcewen, A. S., Dundas, C. M., and Russell, P. S. (2007). Athabasca Valles, Mars: A lava-draped channel system. *Science*, **317**, 1709–1711.

Jellinek, A. M., Johnson, C. L., and Schubert, G. (2008). Constraints on the elastic thickness, heatflow and melt production at early Tharsis from topography and magnetic field observations. *J. Geophys. Res.*, **113**, E09004, doi:10.1029/2007JE003005.

Johnson, C. L. and Phillips, R. J. (2005). Evolution of the Tharsis region of Mars: Insights from magnetic field observations. *Earth Planet. Sci. Lett.*, **230**, 241–254.

Kaula, W. M. (1975). The seven ages of a planet. *Icarus*, **26**, 1–15.

Kiefer, W. S., Bills, B. G., and Nerem, R. S. (1996). An inversion of gravity and topography for mantle and crustal structure on Mars. *J. Geophys. Res.*, **101**, 9239–9252.

Kronberg, P., Hauber, E., Grott, M., Werner, S. C., Schäfer, T., Gwinner, K., Giese, B., Masson, P., and Neukum, G. (2007). Acheron Fossae, Mars: Tectonic rifting, volcanism, and implications for lithospheric thickness. *J. Geophys. Res.*, **112**, doi:10.1029/2006JE002780.

Langlais, B., Purucker, M. E., and Mandea, M. (2004). Crustal magnetic field of Mars. *J. Geophys. Res.*, **109**, doi:10.1029/2003JE002048.

Lee, D.-C. and Halliday, A. N. (1997). Core formation on Mars and differentiated asteroids. *Nature*, **388**, 854–857.

Lemoine, F. G., Smith, D. E., Rowlands, D. D., Zuber, M. T., Neumann, G. A., Chinn, D. S., and Pavlis, D. E. (2001). An improved solution of the gravity field of Mars (GMM-2B) from Mars Global Surveyor. *J. Geophys. Res.*, **106**, 23 359–23 376.

Lenardic, A., Nimmo, F., and Moresi, L. (2004). Growth of the hemispheric dichotomy and the cessation of plate tectonics on Mars. *J. Geophys. Res.*, **109**, doi:10.1029/2003JE002172.

Leonard, G. J. and Tanaka, K. L. (2001). Geologic map of the Hellas region of Mars. U.S. Geol. Surv. Geol. Invest. Ser., Map I-2694.

Lopes, R. M., Guest, J. E., and Wilson, C. J. N. (1980). Origin of the Olympus Mons aureole and perimeter scarp. *Moon and Planets*, **22**, 221–234.

Lopes, R. M., Guest, J. E., Hiller, K., and Neukum, G. (1982). Further evidence for a mass movement origin for the Olympus Mons aureole. *J. Geophys. Res.*, **87**, 9917–9928.

Lowry, A. R. and Zhong, S. (2003). Surface versus internal loading of the Tharsis rise. *J. Geophys. Res.*, **108**, doi:10.1029/2003JE002111.

Lucchitta, B. K., McEwen, A. S., Clow, C. D., Geissler, R. B., Singer, R. B., Schultz, R. A., and Squyres, S. W. (1992). The canyon system on Mars. In *Mars*, ed. H. H. Kieffer, B. M. Jakosky, C. W. Snyder and M. S. Matthews. Tucson, AZ: University of Arizona Press.

Mangold, N., Allemand, P., and Thomas, P. G. (1998). Wrinkle ridges of Mars: Structural analysis and evidence for shallow deformation controlled by ice-rich decollements. *Planet. Space Sci.*, **46**, 345–356.

Mangold, N., Allemand, P., Thomas, P. G., and Vidal, G. (2000). Chronology of compressional deformation on Mars: Evidence for a single and global origin. *Planet. Space Sci.*, **48**, 1201–1211.

Marinova, M. M., Aharonson, O., and Asphaug, E. (2008). Mega-impact formation of the Mars hemispheric dichotomy. *Nature*, **453**, 1216–1219.

Masson, P. (1977). Structure pattern analysis of the Noctis Labyrinthus-Valles Marineris regions of Mars. *Icarus*, **30**, 49–62.

Matsuyama, I., Mitrovica, J. X., Manga, M., Perron, J. T., and Richards, M. A. (2006). Rotational stability of dynamic planets with elastic lithospheres. *J. Geophys. Res.*, **111**, doi:10.1029/2005JE002447.

Maxwell, T. A. (1982). Orientation and origin of ridges in the Lunae Palus-Coprates region of Mars. *Proc. Lunar Planet. Sci. Conf. 13 J. Geophys. Res.*, **87**, A97-A108.

Maxwell, T. A. and McGill, G. E. (1988). Ages of fracturing and resurfacing in the Amenthes region, Mars. *Proc. Lunar Planet. Sci. Conf. 18*, 701–711.

McEwen, A. S., Malin, M. C., Carr, M. H., and Hartmann, W. K. (1999). Voluminous volcanism on early Mars revealed in Valles Marineris. *Nature*, **397**, 584–586.

McGill, G. E. and Dimitriou, A. M. (1990). Origin of the Martian global dichotomy by crustal thinning in the Late Noachian or Early Hesperian. *J. Geophys. Res.*, **95**, 2573–2759.

McGill, G. E. and Squyres, S. W. (1991). Origin of the Martian crustal dichotomy: Evaluating hypotheses. *Icarus*, **93**, 386–393.

McGovern, P. J. and Solomon, S. C. (1993). State of stress, faulting and eruption characteristics of large volcanoes on Mars. *J. Geophys. Res.*, **98**, 23 553–23 579.

McGovern, P. J., Solomon, S. C., Smith, D. E., Zuber, M. T., Simons, M., Wieczorek, M. A., Phillips, R. J., Neumann, G. A., Aharonson, O., and Head, J. W. (2002). Localized gravity/topography admittance and correlation spectra on Mars: Implications for regional and global evolution. *J. Geophys. Res.*, **107**, doi:10.1029/2002JE001854.

McGovern, P. J., Smith, J. R., Morgan, J. K., and Bulmer, M. H. (2004a). Olympus Mons aureole deposits: New evidence for a flank failure origin. *J. Geophys. Res.*, **109**, doi:10.1029/2004JE002258.

McGovern, P. J., Solomon, S. C., Smith, D. E., Zuber, M. T., Simons, M., Wieczorek, M. A., Phillips, R. J., Neumann, G. A., Aharonson, O., and Head, J. W. (2004b). Correction to "Localized gravity/topography admittance and correlation spectra on Mars: Implications for regional and global evolution." *J. Geophys. Res.*, **109**, doi:10.1029/2004JE002286.

McKenzie, D. and Nimmo, F. (1999). The generation of Martian floods by the melting of ground ice above dykes. *Nature*, **397**, 231–233.

McKenzie, D., Barnett, D. N., and Yuan, D.-N. (2002). The relationship between Martian gravity and topography. *Earth Planet. Sci. Lett.*, **195**, 1–16.

McNutt, M. K. (1984). Lithospheric flexure and thermal anomalies. *J. Geophys. Res.*, **89**, 11 180–11 194.

Mege, D. and Masson, P. (1996a). A plume tectonics model for the Tharsis Province, Mars. *Planet. Space Sci.*, **44**, 1499–1546.

Mege, D. and Masson, P. (1996b). Amounts of crustal stretching in Valles Marineris, Mars. *Planet. Space Sci.*, **44**, 749–781.

Mege, D., Cook, A. C., Garel, E., Lagabrielle, Y., and Cormier, M. H. (2003). Volcanic rifting at Martian grabens. *J. Geophys. Res.*, **108**, doi:10.1029/2002JE001852.

Melosh, H. J. (1980). Tectonic patterns on a reoriented planet: Mars. *Icarus*, **44**, 745–751.

Milbury, C. A. E., Smrekar, S. E., Raymond, C. A., and Schubert, G. (2007). Lithospheric structure in the eastern region of Mars' dichotomy boundary. *Planet. Space Sci.*, **55**, 280–288.

Mitchell, D. L., Lillis, R. J., Lin, R. P., Connerney, J. E. P., and Acuña, M. H. (2007). A global map of Mars' crustal magnetic field based on electron reflectometry. *J. Geophys. Res.*, **112**, doi:10.1029/2005JE002564.

Montesi, L. G. J. and Zuber, M. T. (2003). Clues to the lithospheric structure of Mars from wrinkle ridge sets and localization instability. *J. Geophys. Res.*, **108**, doi:10.1029/2002JE001974.

Moore, H. J. (2001). Geologic map of the Tempe-Mareotis region of Mars. U.S. Geol. Surv. Geol. Invest. Ser., Map I-2727.

Morris, E. C. and Tanaka, K. L. (1994). Geologic maps of the Olympus Mons region of Mars. U.S. Geol. Surv. Misc. Invest. Ser., Map I-2327-B.

Mouginis-Mark, P. J. (1981). Late-stage summit activity of Martian shield volcanoes. *Proc. Lunar Planet. Sci. Conf. 12*, 1431–1447.

Mouginis-Mark, P. J., Wilson, L., Head, J. W., Brown, S. H., Hall, J. L., and Sullivan, K. (1984). Elysium Planitia, Mars: Regional geology, volcanology, and evidence for volcano-ground interactions. *Earth, Moon and Planets*, **30**, 149–173.

Mueller, K. and Golombek, M. P. (2004). Compressional structures on Mars. *Annu. Rev. Earth Planet. Sci.*, **32**, 435–464, doi:10.1146/annurev.earth.32.101802.120553.

Mustard, J. F., Murchie, S. L., Pelkey, S. M., Ehlmann, B. L., Milliken, R. E., Grant, J. A., Bibring, J.-P., Poulet, F., Bishop, J., Noe Dobrea, E., Roach, L., Seelos, F., Arvidson, R. E., Wiseman, S., Green, R., Hash, C., Humm, D., Malaret, E., McGovern, J. A., Seelos, K., Clancy, T., Clark, R., Des Marais, D., Izenberg, N., Knudson, A., Langevin, Y., Martin, T., McGuire, P., Morris, R., Robinson, M., Roush, T., Smith, M., Swayze, G., Taylor, H., Titus, T., and Wolff, M. (2008). Hydrated silicate minerals on Mars observed by the Mars Reconnaissance Orbiter CRISM instrument. *Nature*, **454**, 305–309.

Neumann, G. A., Zuber, M. T., Wieczorek, M. A., McGovern, P. J., Lemoine, F. G., and Smith, D. E. (2004). Crustal structure of Mars from gravity and topography. *J. Geophys. Res.*, **109**, E08002, doi:10.1029/2004JE002262.

Neumann, G. A., Lemoine, F. G., Smith, D. E., and Zuber, M. T. (2008). Marscrust3-a crustal thickness inversion from recent MRO gravity solutions (abs.). *Lunar Planet. Sci. Conf. XXXIX*, 2167. Houston, TX: Lunar and Planetary Institute (CD-ROM).

Nimmo, F. (2002). Admittance estimates of mean crustal thickness and density at the Martian hemispheric dichotomy. *J. Geophys. Res.*, **107**, doi:10.1029/2000JE001488.

Nimmo, F. (2005). Tectonic consequences of Martian dichotomy modification by lower-crustal flow and erosion. *Geology*, **33**, 533–536.

Nimmo, F. and Stevenson, D. J. (2001). Estimates of Martian crustal thickness from viscous relaxation of topography. *J. Geophys. Res.*, **106**, 5085–5098.

Nimmo, F. and Tanaka, K. L. (2005). Early crustal evolution of Mars. *Annu. Rev. Earth Planet. Sci.*, **33**, 133–161.

Nimmo, F., Hart, S. D., Korycansky, D. G., and Agnor, C. B. (2008). Implications of an impact origin for the Martian hemispheric dichotomy. *Nature*, **453**, 1220–1223.

Okubo, C. H. and Schultz, R. A. (2003). Thrust fault vergence directions on Mars: A foundation for investigating global-scale Tharsis-driven tectonics. *Geophys. Res. Lett.*, **30**, 2154, doi:10.1029/2003GL018664.

Okubo, C. H. and Schultz, R. A. (2004). Mechanical stratigraphy in the western equatorial region of Mars based on thrust fault-related fold topography and implications for near-surface volatile reservoirs. *GSA Bulletin*, **116**, 594–605, doi:10.1130/B25361.1.

Okubo, C. H. and Schultz, R. A. (2006). Variability in Early Amazonian Tharsis stress state based on wrinkle ridges and strike-slip faulting. *J. Struct. Geol.*, **28**, 2169–2181.

Perron, J. T., Mitrovica, J. X., Manga, M., Matsuyama, I., and Richards, M. A. (2007). Evidence for an ancient Martian ocean in the topography of deformed shorelines. *Nature*, **447**, 840–843.

Peulvast, J. P. and Masson, P. L. (1993a). Erosion and tectonics in central Valles Marineris (Mars): A new morpho-structural model. *Earth, Moon and Planets*, **61**, 191–217.

Peulvast, J. P. and Masson, P. L. (1993b). Melas Chasma: Morphology and tectonic patterns in central Valles Marineris (Mars). *Earth, Moon and Planets*, **61**, 219–248.

Phillips, R. J. and Lambeck, K. (1980). Gravity fields of the terrestrial planets: Long-wavelength anomalies and tectonics. *Rev. Geophys. Space Phys.*, **18**, 27–76.

Phillips, R. J., Saunders, R. S., and Conel, J. E. (1973). Mars: Crustal structure inferred from Bouguer gravity anomalies. *J. Geophys. Res.*, **78**, 4815–4820.

Phillips, R. J., Sleep, N. H., and Banerdt, W. B. (1990). Permanent uplift in magmatic systems with application to the Tharsis region of Mars. *J. Geophys. Res.*, **95**, 5089–5100.

Phillips, R. J., Zuber, M. T., Solomon, S. C., Golombek, M. P., Jakosky, B. M., Banerdt, W. B., Smith, D. E., Williams, R. M. E., Hynek, B. M., Aharonson, O., and Hauck I, S. A. (2001). Ancient geodynamics and global-scale hydrology on Mars. *Science*, **291**, 2587–2591.

Phillips, R. J., Johnson, C. L., and Dombard, A. J. (2004). Localized Tharsis loading on Mars: Testing the membrane surface hypothesis (abs.). *Lunar Planet Sci. Conf. XXXV*, 1427. Houston, TX: Lunar and Planetary Institute (CD-ROM).

Phillips, R. J., Zuber, M. T., Smrekar, S. E., Mellon, M. T., Head, J. W., Tanaka, K. L., Putzig, N. E., Milkovich, S. M., Campbell, B. A., Plaut, J. J., Safaeinili, A., Seu, R., Biccari, D., Carter, L. M., Picardi, G., Orosei, R., Mohit, P. S., Heggy, E., Zurek, R. W., Egan, A., Giacomoni, E., Russo, F., Cutigni, M., Pettinelli, E., Holt, J. W., Leuschen, C. J., and Marinangeli, L. (2008). Mars north polar deposits: Stratigraphy, age and geodynamical response. *Science*, **230**, 1182–1185.

Plescia, J. B. (1991a). Graben and extension in northern Tharsis, Mars. *J. Geophys. Res.*, **96**, 18 883–18 895.

Plescia, J. B. (1991b). Wrinkle ridges in Lunae Planum, Mars: Implications for shortening and strain. *Geophys. Res. Lett.*, **18**, 913–916.

Plescia, J. B. (1993). Wrinkle ridges of Arcadia Planitia, Mars. *J. Geophys. Res.*, **98**, 15 049–15 059.

Plescia, J. B. and Golombek, M. P. (1986). Origin of planetary wrinkle ridges based on the study of terrestrial analogs. *Geol. Soc. Am. Bull.*, **97**, 1289–1299.

Plescia, J. B. and Saunders, R. S. (1982). Tectonic history of the Tharsis Region, Mars. *J. Geophys. Res.*, **87**, 9775–9791.

Pruis, M. J. and Tanaka, K. L. (1995). The Martian northern plains did not result from plate tectonics (abs.). *Lunar Planet. Sci. Conf. XXVI*. Houston, TX: Lunar and Planetary Institute, 1147–1148.

Purucker, M., Ravat, D., Frey, H., Voorhies, C., Sabaka, T., and Acuña, M. (2000). An altitude-normalized magnetic map of Mars and its interpretation. *Geophys. Res. Lett.*, **27**, 2449–2452.

Quesnel, Y., Langlais, B., and Sotin, C. (2007). Local inversion of magnetic anomalies: Implication for Mars' crustal evolution. *Planet. Space Sci.*, **55**, 258–269.

Raitala, J. (1988). Superposed ridges of the Hesperia Planum Area on Mars. *Earth, Moon and Planets*, **40**, 71–99.

Raitala, J. and Kauhanen, K. (1989). Tectonics of Syrtis Major Planum on Mars. *Earth, Moon and Planets*, **46**, 243–260.

Redmond, H. L. and King, S. D. (2004). A numerical study of a mantle plume beneath the Tharsis Rise: Reconciling dynamic uplift and lithospheric support models. *J. Geophys. Res.*, **109**, doi:10.1029/2003JE002228.

Reese, C. C., Solomatov, V. S., Baumgardner, J. R., Stegman, D. R., and Vezolainen, A. V. (2004). Magmatic evolution of impact-induced Martian mantle plumes and the origin of Tharsis. *J. Geophys. Res.*, **109**, doi:10.1029/2003JE002222.

Roberts, J. H. and Zhong, S. (2004). Plume-induced topography and geoid anomalies and their implications for the Tharsis rise on Mars. *J. Geophys. Res.*, **109**, doi:10.1029/2003JE002226.

Roberts, J. H. and Zhong, S. (2006). Degree-1 convection in the Martian mantle and the origin of the hemispheric dichotomy. *J. Geophys. Res.*, **111**, doi:10.1029/2005JE002668.

Roberts, J. H. and Zhong, S. (2007). The cause for the north–south orientation of the crustal dichotomy and the equatorial location of Tharsis on Mars. *Icarus*, **190**, 24–31.

Sandwell, D. T., Johnson, C. L., Bilotti, F., and Suppe, J. (1997). Driving forces for limited tectonics on Venus. *Icarus*, **129**, 232–244.

Schubert, G., Solomon, S. C., Turcotte, D. L., Drake, M. J., and Sleep, N. H. (1992). Origin and thermal evolution of Mars. In *Mars*, ed. H. H. Kieffer, B. M. Jakosky, C. W. Snyder and M. S. Matthews. Tucson, AZ: University of Arizona Press, pp. 147–183.

Schultz, R. A. (1989). Strike-slip faulting of ridged plains near Valles Marineris, Mars. *Nature*, **341**, 424–428.

Schultz, R. A. (1991). Structural development of Coprates Chasma and western Ophir Planum. *J. Geophys. Res.*, **96**, 22 777–22 792.

Schultz, R. A. (1995). Gradients in extension and strain at Valles Marineris. *Planet. Space Sci.*, **43**, 1561–1566.

Schultz, R. A. (1998). Multiple-process origin of Valles Marineris basins and troughs. *Planet. Space Sci.*, **46**, 827–834.

Schultz, R. A. (2000). Localization of bedding-plane slip and backthrust faults above blind thrust faults: Keys to wrinkle ridge structure. *J. Geophys. Res.*, **105**, 12 035–12 052.

Schultz, R. A. and Lin, J. (2001). Three-dimensional normal faulting models of Valles Marineris, Mars, and geodynamic implications. *J. Geophys. Res.*, **106**, 16 549–16 566.

Schultz, R. A. and Tanaka, K. L. (1994). Lithospheric-scale buckling and thrust structures on Mars: The Coprates rise and south Tharsis ridge belt. *J. Geophys. Res.*, **99**, 8371–8385.

Schultz, R. A., Okubo, C. H., Goudy, C. L., and Wilkins, S. J. (2004). Igneous dikes on Mars revealed by Mars Orbiter Laser Altimeter topography. *Geology*, **32**, 889–892.

Schultz, R. A., Moore, J. M., Grosfils, E. B., Tanaka, K. L., and Mège, D. (2007). The Canyonlands model for planetary grabens: Revised physical basis and implications. In *The Geology of Mars: Evidence from Earth-Based Analogs*, ed. M. Chapman. Cambridge: Cambridge University Press, pp. 371–399.

Scott, D. H. and Dohm, J. M. (1990a). Chronology and global distribution of fault and ridge systems on Mars. *Proc. Lunar Planet. Sci. Conf. 20*. Houston, TX: Lunar and Planetary Institute, 487–501.

Scott, D. H. and Dohm, J. M. (1990b). Faults and ridges: Historical development in Tempe Terra and Ulysses Patera regions of Mars. *Proc. Lunar Planet. Sci. Conf. 20.* Houston, TX: Lunar and Planetary Institute, 503–513.

Scott, D. H. and Tanaka, K. L. (1986). Geologic map of the western equatorial region of Mars. U.S. Geol. Surv. Map I-1802-A.

Scott, E. D. and Wilson, L. (2002). Plinian eruptions and passive collapse events as mechanisms of formation for Martian pit chain craters. *J. Geophys. Res.*, **107**, doi:10.1029/2000JE001432.

Scott, E. D., Wilson, L., and Head III, J. W. (2002). Emplacement of giant radial dikes in the northern Tharsis region of Mars. *J. Geophys. Res.*, doi:10.1029/2000JE001431.

Searls, M. L. and Phillips, R. J. (2007). Tectonics of Utopia Basin, Mars: Results from finite element loading models (abs.). *Lunar Planet. Sci. Conf. XXXVIII*, 1965. Houston, TX: Lunar and Planetary Institute (CD-ROM).

Searls, M. L., Banerdt, W. B., and Phillips, R. J. (2006). Utopia and Hellas basins, Mars: Twins separated at birth. *J. Geophys. Res.*, **111**, doi:10.1029/2005JE002666.

Segura, T. L., Toon, O. B., Colaprete, A., and Zahnle, K. (2002). Environmental effects of large impacts on Mars. *Science*, **298**, 1977–1980.

Sleep, N. H. (1994). Martian plate tectonics. *J. Geophys. Res.*, **99**, 5639–5655.

Sleep, N. H. and Tanaka, K. L. (1995). Point-counterpoint: Did Mars have plate tectonics? *Mercury*, **24**, 10–11.

Smith, D. E., Sjogren, W. L., Tyler, G. L., Balmino, G., Lemoine, F. G., and Konopliv, A. S. (1999a). The gravity field of Mars: Results from Mars Global Surveyor. *Science*, **286**, 94–97.

Smith, D. E., Zuber, M. T., Solomon, S. C., Phillips, R. J., Head, J. W., Garvin, J. B., Banerdt, W. B., Muhleman, D. O., Pettingill, G. H., Neumann, G. A., Lemoine, F. G., Abshire, J. B., Aharonson, O., Brown, C. D., Hauck II, S. A., Ivanov, A. B., McGovern, P. J., Zwally, H. J., and Duxbury, T. C. (1999b). The global topography of Mars and implications for surface evolution. *Science*, **284**, 1495–1503.

Smith, D. E., Zuber, M. T., Frey, H. V., Garvin, J. B., Head, J. W., Muhleman, D. O., Pettingill, G. H., Phillips, R. J., Solomon, S. C., Zwally, H. J., Banerdt, W. B., Duxbury, T. C., Golombek, M. P., Lemoine, F. G., Neumann, G. A., Rowlands, D. D., Aharonson, O., Ford, P. G., Ivanov, A. B., Johnson, C. L., McGovern, P. J., Abshire, J. B., Afzal, R. S., and Sun, X. (2001). Mars Orbiter Laser Altimeter (MOLA): Experiment summary after the first year of global mapping of Mars. *J. Geophys. Res.*, **106**, 23 689–23 722.

Smrekar, S. E., McGill, G. E., Raymond, C. A., and Dimitriou, A. M. (2004). Geologic evolution of the Martian dichotomy in the Ismenius area of Mars and implications for plains magnetization. *J. Geophys. Res.*, **109**, doi:10.1029/2004JE002260.

Solomon, S. C. and Head, J. W. (1980). Lunar mascon basins: Lava filling, tectonics, and evolution of the lithosphere. *Rev. Geophys.*, **18**, 107–141.

Solomon, S. C. and Head, J. W. (1982). Evolution of the Tharsis province of Mars: The importance of heterogeneous lithospheric thickness and volcanic construction. *J. Geophys. Res.*, **87**, 9755–9774.

Solomon, S. C. and Head, J. W. (1990). Heterogeneities in the thickness of the elastic lithosphere of Mars: Constraints on heat flow and internal dynamics. *J. Geophys. Res.*, **95**, 11 073–11 083.

Solomon, S. C., Aharonson, O., Aurnou, J. M., Banerdt, W. B., Carr, M. H., Dombard, A. J., Frey, H. V., Golombek, M. P., Hauck II, S. A., Head III, J. W., Jakosky, B. M., Johnson, C. L., McGovern, P. J., Neumann, G. A., Phillips, R. J., Smith, D. E., and Zuber, M. T. (2005). New perspectives on ancient Mars. *Science*, **307**, 1214–1220.

Solomon, S. C., McNutt Jr., R. L., Watters, T. R., Lawrence, D. J., Feldman, W. C., Head, J. W., Krimigis, S. M., Murchie, S. L., Phillips, R. J., Slavin, J. A., and Zuber, M. T. (2008). Return to Mercury: A global perspective on MESSENGER's first Mercury flyby. *Science*, **321**, 59–62.

Spohn, T., Acuña, M. H., Breuer, D., Golombek, M. P., Greeley, R., Halliday, A., Hauber, E., Jaumann, R., and Sohl, F. (2001). Geophysical constraints on the evolution of Mars. *Space Sci. Rev.*, **96**, 231–262.

Sprenke, K. F., Baker, L. L., and Williams, A. F. (2005). Polar wander on Mars: Evidence in the geoid. *Icarus*, **174**, 486–489.

Squyres, S. W., Grotzinger, J. P., Arvidson, R. E., Bell III, J. F., Calvin, W., Christensen, P. R., Clark, B. C., Crisp, J. A., Farrand, W. H., Herkenhoff, K. E., and Johnson, J. R. (2004). In-situ evidence for an ancient aqueous environment at Meridiani Planum, Mars. *Science*, **306**, 1709–1714.

Squyres, S. W., Arvidson, R. E., Blaney, D. L., Clark, B. C., Crumpler, L., Farrand, W. H., Gorevan, S., Herkenhoff, K. E., Hurowitz, J., Kusack, A., McSween, H. Y., Ming, D. W., Morris, R. V., Ruff, S. W., Wang, A., and Yen, A. (2006). Rocks of the Columbia Hills. *J. Geophys. Res.*, **111**, doi:10.1029/2005JE002562.

Suppe, J. and Medwedeff, D. A. (1990). Geometry and kinematics of fault-propagation folding. *Eclogae Geo. Helv.*, **83**, 409–454.

Tanaka, K. L. (1985). Ice-lubricated gravity spreading of the Olympus Mons aureole deposits. *Icarus*, **62**, 191–206.

Tanaka, K. L. (1986). The stratigraphy of Mars. *Proc. Lunar and Planet. Sci. Conf. 17. J. Geophys. Res.*, **91**, E139–E158.

Tanaka, K. L. (1990). Tectonic history of the Alba Patera-Ceraunius Fossae region of Mars. *Proc. Lunar Planet. Sci. Conf. 20*. Houston, TX: Lunar and Planetary Institute, 515–523.

Tanaka, K. L. and Chapman, M. G. (1990). The relation of catastrophic flooding of Mangala Valles, Mars, to faulting of Menmonia Fossae and Tharsis volcanism. *J. Geophys. Res.*, **95**, 14 315–14 323.

Tanaka, K. L. and Davis, P. A. (1988). Tectonic history of the Syria Planum province of Mars. *J. Geophys. Res.*, **93**, 14 893–14 917.

Tanaka, K. L. and Golombek, M. P. (1989). Martian tension fractures and the formation of grabens and collapse features at Valles Marineris. *Proc. Lunar Planet. Sci. Conf. 19*, 383–396.

Tanaka, K. L. and Hartmann, W. K. (2008). The planetary timescale. *The Concise Geologic Time Scale*, ed. J. G. Ogg, G. M. Ogg and F. M. Gradstein. New York: Cambridge University Press, pp. 13–22.

Tanaka, K. L. and Leonard, G. J. (1995). Geology and landscape evolution of the Hellas region of Mars. *J. Geophys. Res.*, **100**, 5407–5432.

Tanaka, K. L., Golombek, M. P., and Banerdt, W. B. (1991). Reconciliation of stress and structural histories of the Tharsis region of Mars. *J. Geophys. Res.*, **96**, 15 617–15 633.

Tanaka, K. L., Skinner Jr., J. A., Hare, T. M., Joyal, T., and Wenker, A. (2003). Resurfacing history of the northern plains of Mars based on geologic mapping of Mars Global Surveyor data. *J. Geophys. Res.*, **108**, doi:10.1029/2002JE001908.

Tanaka, K. L., Skinner Jr., J. A., and Hare, T. M. (2005). Geologic map of the northern plains of Mars. U.S. Geol. Surv., Map SIM-2888.

Tate, A., Mueller, K., and Golombek, M. P. (2002a). Kinematics and structural inversion of wrinkle ridges on Lunae and Solis Planum: Implications for the early history of Tharsis (abs.). *Lunar Planet. Sci. Conf. XXXIII*, 1828. Houston, TX: Lunar and Planetary Institute (CD-ROM).

Tate, A., Mueller, K. J., and Golombek, M. P. (2002b). Geometry and kinematics of wrinkle ridges on Lunae and Solis Planum: Implications for fault/fold growth history (abs.). *Lunar Planet. Sci. Conf. XXXIII*, 1836. Houston, TX: Lunar and Planetary Institute (CD-ROM).

Thomas, P. G. and Allemand, P. (1993). Quantitative analysis of the extensional tectonics of the Tharsis bulge, Mars: Geodynamic implications. *J. Geophys. Res.*, **98**, 13 097–13 108.

Thomas, P. J., Squyres, S. W., and Carr, M. H. (1990). Flank tectonics of Martian volcanoes. *J. Geophys. Res.*, **95**, 14 345–14 355.

Thomson, B. J. and Head, J. W. (2001). Utopia basin, Mars: Characterization of topography and morphology and assessment of the origin and evolution of basin internal structure. *J. Geophys. Res.*, **106**, 23 209–23 230.

Turcotte, D. L., Willemann, R. J., Haxby, W. F., and Norberry, J. (1981). Role of membrane stress in the support of planetary topography. *J. Geophys. Res.*, **86**, 3951–3959.

van Thienen, P., Rivoldini, A., Van Hoolst, T., and Lognonné, P. (2006). A top-down origin for Martian mantle plumes. *Icarus*, **185**, 197–210.

Vidal, A., Mueller, K., and Golombek, M. P. (2003). Axial surface mapping of wrinkle ridges on Solis Planum, Mars from MOLA topography: Constraints on subsurface blind thrust geometry (abs.). *Lunar Planet. Sci. Conf. XXXIV*, 1125. Houston, TX: Lunar and Planetary Institute (CD-ROM).

Vidal, A., Mueller, K. M., and Golombek, M. P. (2005). Geometry of thrust faults beneath Amenthes Rupes, Mars (abs.). *Lunar Planet. Sci. Conf. XXXVI*, 2333. Houston, TX: Lunar and Planetary Institute (CD-ROM).

Vlasov, V. Z. (1964). *General Theory of Shells and Its Applications in Engineering.* NASA Tech. Trans. T T F-99.

Ward, P. D. and Brownlee, D. (2000). *Rare Earth*. New York: Springer-Verlag.

Ward, P. D. and Brownlee, D. (2002). *The Life and Death of Planet Earth*. New York: H. Holt.

Watters, T. R. (1988). Wrinkle ridge assemblages on the terrestrial planets. *J. Geophys. Res.*, **93**, 10 236–10 254.

Watters, T. R. (1991). Origin of periodically spaced wrinkle ridges on the Tharsis Plateau of Mars. *J. Geophys. Res.*, **96**, 15 599–15 616.

Watters, T. R. (1992). System of tectonic features common to Earth, Mars, and Venus. *Geology*, **20**, 609–612.

Watters, T. R. (1993). Compressional tectonism on Mars. *J. Geophys. Res.*, **98**, 17 049–17 060.

Watters, T. R. (2003a). Lithospheric flexure and the origin of the dichotomy boundary on Mars. *Geology*, **31**, 271–274.

Watters, T. R. (2003b). Thrust faults along the dichotomy boundary in the eastern hemisphere of Mars. *J. Geophys. Res.*, **108**, doi:10.1029/2002JE001934.

Watters, T. R. (2004). Elastic dislocation modeling of wrinkle ridges on Mars. *Icarus*, **171**, 284–294.
Watters, T. R. and Maxwell, T. A. (1986). Orientation, relative age, and extent of the Tharsis plateau ridge system. *J. Geophys. Res.*, **91**, 8113–8125.
Watters, T. R. and Robinson, M. S. (1997). Radar and photoclinometric studies of wrinkle ridges on Mars. *J. Geophys. Res.*, **102**, 10 889–10 903.
Watters, T. R., Schultz, R. A., and Robinson, M. S. (2000). Displacement–length relations of thrust faults associated with lobate scarps on Mercury and Mars: Comparison with terrestrial faults. *Geophys. Res. Lett.*, **27**, 3659–3662.
Weissel, J. K. and Karner, G. D. (1989). Flexural uplift of rift flanks due to mechanical unloading of the lithophere during extension. *J. Geophys. Res.*, **94**, 13 919–13 950.
Wenzel, M. J., Manga, M., and Jellinek, A. M. (2004). Tharsis as a consequence of Mars' dichotomy and layered mantle. *Geophys. Res. Lett.*, **31**, doi:10.1029/2003GL019306.
Wichman, R. W. and Schultz, P. H. (1989). Sequence and mechanisms of deformation around the Hellas and Isidis impact basins on Mars. *J. Geophys. Res.*, **94**, 17 333–17 357.
Wieczorek, M. A. and Zuber, M. T. (2004). Thickness of the Martian crust: Improved constraints from geoid-to-topography ratios. *J. Geophys. Res.*, **109**, doi:01010.01029/02003JE002153.
Wilhems, D. E. and Squyres, S. W. (1984). The Martian hemispheric dichotomy may be due to a giant impact. *Nature*, **309**, 138–140.
Wilkins, S. J. and Schultz, R. A. (2003). Cross faults in extensional settings: Stress triggering, displacements localization, and implications for the origin of blunt troughs at Valles Marineris. *J. Geophys. Res.*, **108**, doi:10.1029/2002JE001968.
Willemann, R. J. (1984). Reorientation of planets with elastic lithospheres. *Icarus*, **60**, 701–709.
Wilson, L. and Head III, J. W. (2002). Tharsis-radial graben systems as the surface manifestation of plume-related dike intrusion complexes: Models and implications. *J. Geophys. Res.*, **107**, doi:10.1029/2001JE001593.
Wise, D. U. (1974). Continental margins, freeboard and the volume of continents and oceans through time. In *The Geology of Continental Margins*, ed. C. A. Burk and C. L. Drake. New York: Springer Verlag, pp. 45–58.
Wise, D. U., Golombek, M. P., and McGill, G. E. (1979). Tharsis province of Mars: Geologic sequence, geometry, and a deformation mechanism. *Icarus*, **38**, 456–472.
Witbeck, N. E., Tanaka, K. L., and Scott, D. H. (1991). Geologic map of the Valles Marineris region, Mars (East Half And West Half): 1:2M. U.S. Geol. Surv. Misc. Invest. Ser., Map I-2010.
Withers, P. and Neumann, G. A. (2001). Enigmatic northern plains of Mars. *Nature*, **410**, 651.
Wyrick, D., Ferrill, D. A., Morris, A. P., Colton, S. L., and Sims, D. W. (2004). Distribution, morphology, and origins of Martian pit crater chains. *J. Geophys. Res.*, **109**, doi:10.1029/2004JE002240.
Yoder, C. F., Konopliv, A. S., Yuan, D. N., Standish, E. M., and Folkner, W. M. (2003). Fluid core size of Mars from detection of the solar tide. *Science*, **300**, 299–303.
Yuan, D. N., Sjogren, W. L., Konopliv, A. S., and Kucinskas, A. B. (2001). Gravity field of Mars: A 75th degree and order model. *J. Geophys. Res.*, **106**, 23 377–23 401.
Zhong, S. (2002). Effects of lithosphere on the long-wavelength gravity anomalies and their implications for the formation of the Tharsis rise on Mars. *J. Geophys. Res.*, **107**, doi:10.1029/2001JE001589.

Zhong, S. and Roberts, J. H. (2003). On the support of the Tharsis rise on Mars. *Earth Planet. Sci. Lett.*, **214**, 1–9.
Zhong, S. and Zuber, M. T. (2001). Degree-1 mantle convection and the crustal dichotomy on Mars. *Earth Planet. Sci. Lett.*, **189**, 75–84.
Zuber, M. T. (1995). Wrinkle ridges, reverse faulting and the depth penetration of lithospheric strain in Lunae Planum, Mars. *Icarus*, **114**, 80–92.
Zuber, M. T. (2001). The crust and mantle of Mars. *Nature*, **412**, 220–227.
Zuber, M. T. and Aist, L. L. (1990). The shallow structure of the Martian lithosphere in the vicinity of the ridged plains. *J. Geophys. Res.*, **95**, 14 215–14 230.
Zuber, M. T. and Mouginis-Mark, P. J. (1992). Caldera subsidence and magma chamber depth of Olympus Mons volcano, Mars. *J. Geophys. Res.*, **97**, 18 295–18 307.
Zuber, M. T. and Smith, D. E. (1997). Mars without Tharsis. *J. Geophys. Res.*, **102**, 28 673–28 685.
Zuber, M. T., Solomon, S. C., Phillips, R. J., Smith, D. E., Tyler, G. L., Aharonson, O., Balmino, G., Banerdt, W. B., Head, J. W., Johnson, C. L., Lemoine, F. G., McGovern, P. J., Neumann, G. A., Rowlands, D. D., and Zhong, S. (2000). Internal structure and early thermal evolution of Mars from Mars Global Surveyor topography and gravity. *Science*, **287**, 1788–1793.
Zuber, M. T., Phillips, R. J., Andrews-Hanna, J. C., Asmar, S. W., Konopliv, A. S., Lemoine, F. G., Plaut, J. J., Smith, D. E., and Smrekar, S. E. (2007). Density of Mars' south polar layered deposits. *Science*, **317**, 1718–1719.

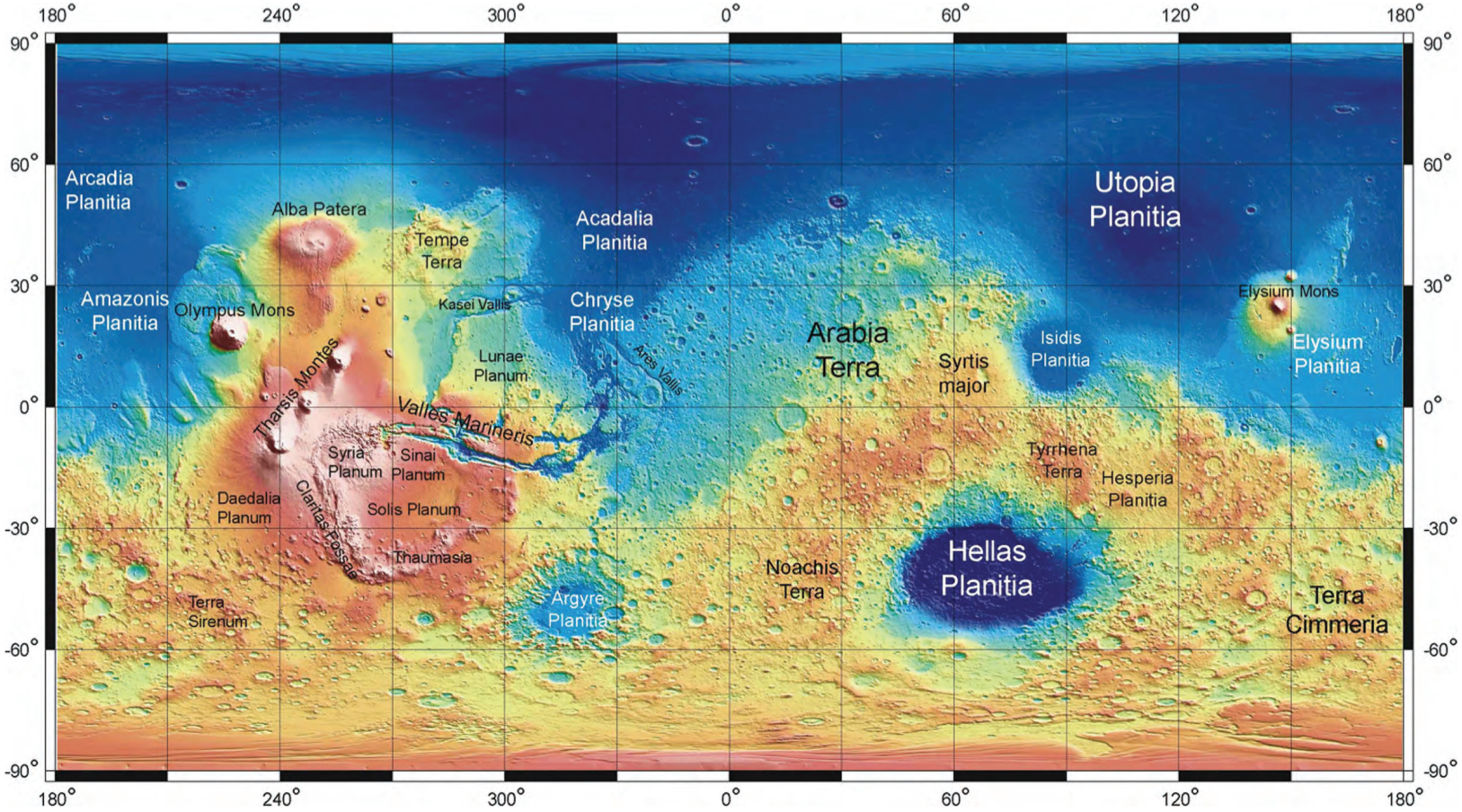

Plate 13. Topographic map and place names for Mars. The elevation range extends from ~ -8 km (blue) to $\sim +8$ km (light pink in Thaumasia and Tharsis rise regions). The Tharsis Montes and Olympus Mons extend to higher elevations. Simple cylindrical projection of MOLA topography.

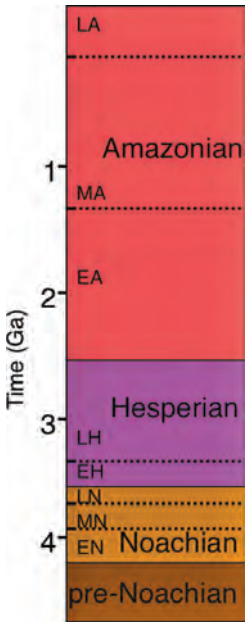

Plate 14. Geologic time scale of Mars based on major geologic/stratigraphic units exposed at the surface (Tanaka, 1986). Absolute time scale is based on correlating crater densities on Mars with radiometrically dated surfaces on the Moon (Hartmann and Neukum, 2001 and references therein; Hartmann, 2005; Tanaka and Hartmann, 2008). Within each era, epochs are shown as Early (EA, EH, EN) and Late (LA, LH, LN), Amazonian, Hesperian and Noachian, respectively. Middle Amazonian (MA) and Noachian (MN) epochs also shown.

Plate 15. Crustal thickness model (Neumann *et al.*, 2008) based on MRO spherical harmonic degree 95 gravity model 95a (A. S. Konopliv). Mean crustal thickness is 45 km and crustal density 2900 kg m^{-3}, with density adjustments made for the Tharsis volcanoes, Elysium Mons, and the polar caps.

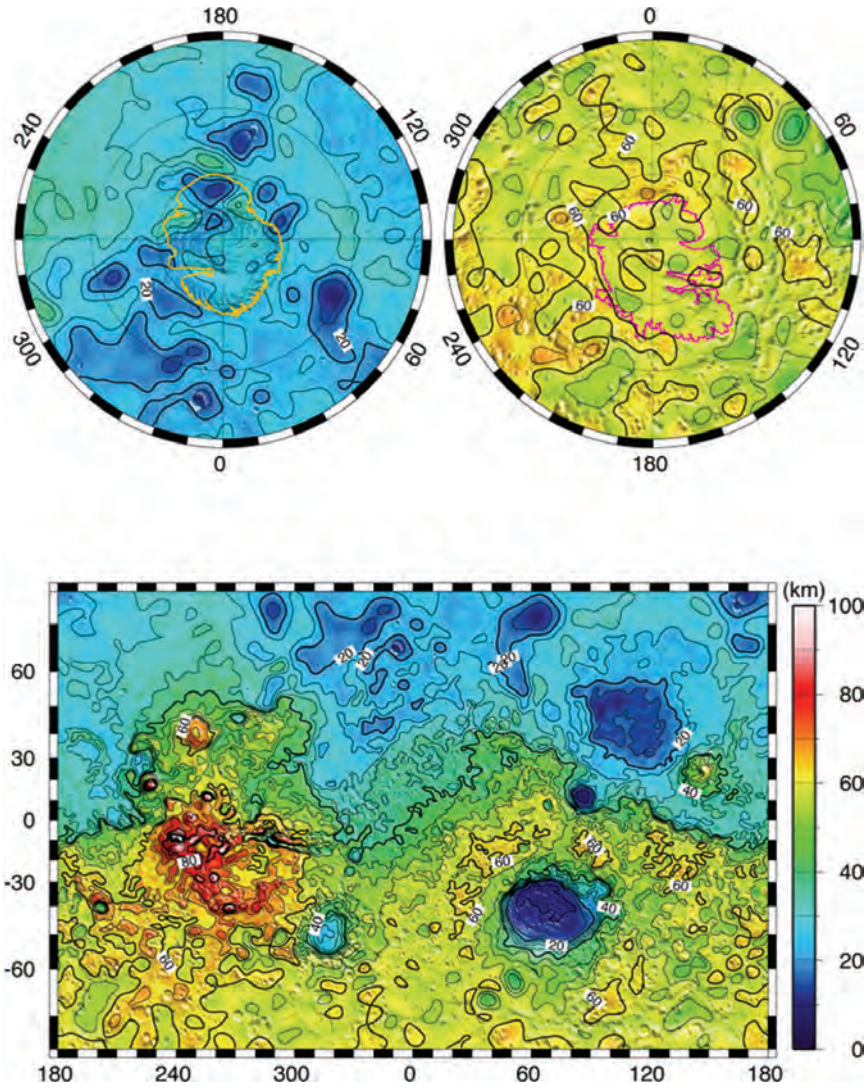

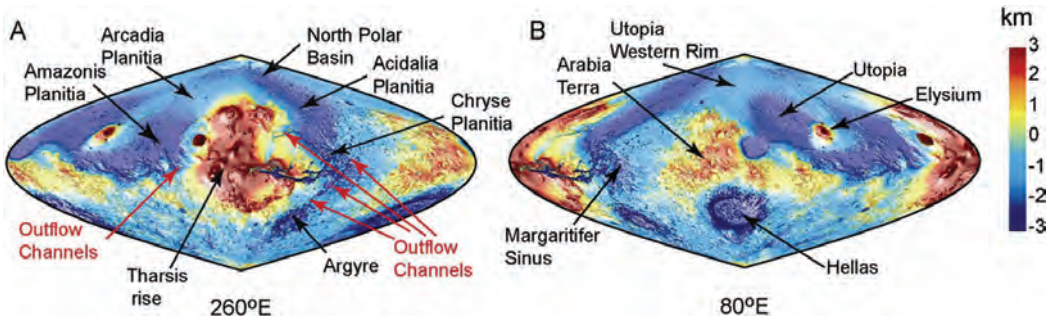

Plate 16. Observed Martian topography for hemisphere centered on Tharsis (A) and the opposite hemisphere (B). The pole-to-pole slope (the J_1 term of a spherical harmonic expansion) has been removed to emphasize other global features. A trough or moat surrounds much of Tharsis and contains most of the planet's outflow channels. To the southwest of Tharsis the trough may be obscured by both Tharsis volcanics and crustal folding. In the other hemisphere, Arabia Terra is the site of a topographic bulge. The trough and bulge are predicted by a model that localizes the Tharsis load on an elastic lithospheric shell (Phillips *et al.*, 2001). Sinusoidal projection.

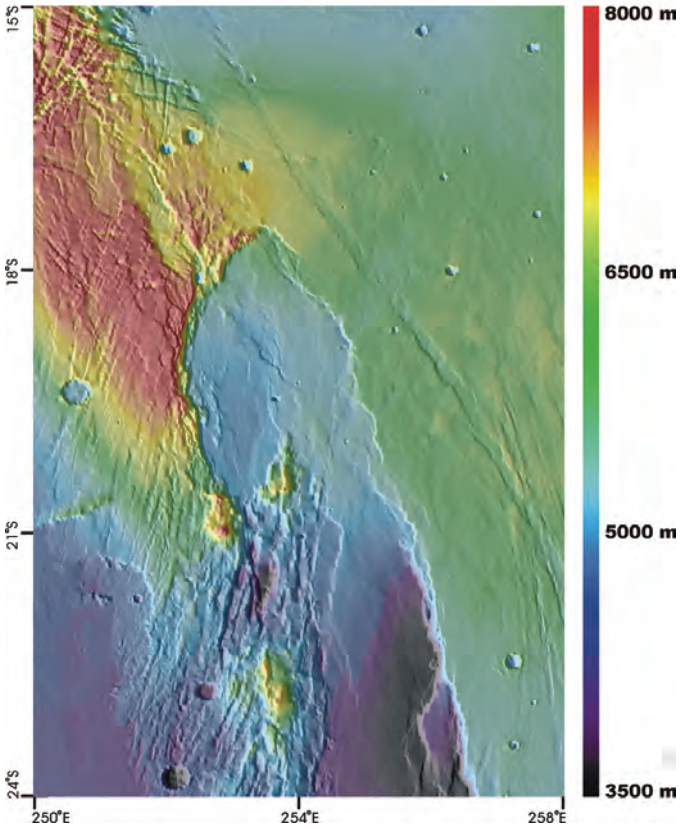

Plate 17. MOLA topographic, shaded relief map of the Thaumasia rift, analogous to a continental rift on Earth, in Claritas Fossae, Mars. The rift is 100–200 km wide with 1–2 km of relief. Note segmented nature of the rift, with the floor north of the intrarift horst tilted into the master fault on the west and the southern floor tilted into the master fault on the east. The north–northeast trending fault set is mapped as Early Hesperian in age, compared with the major rifting, which occurred in the Early Amazonian (Tanaka and Davis, 1988). The older fault set was clearly reactivated during rifting. The 360-km wide map is derived from the 0.5 km gridded MOLA elevations (Smith *et al.*, 2001), illuminated from the west.

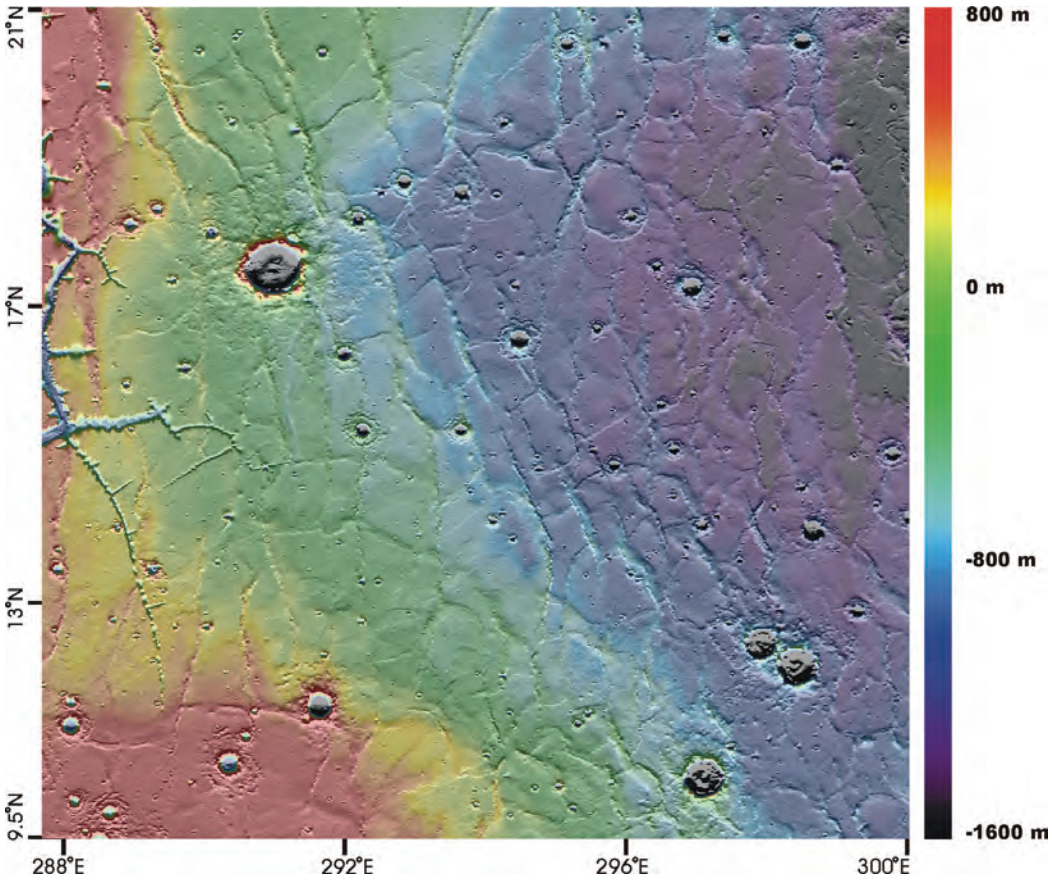

Plate 18. MOLA topographic, shaded relief map of Lunae Planum showing the classic ridged plains on Mars. Wrinkle ridges show up prominently as positive relief hills with sharper wrinkles or crenulations. The primary regularly spaced set of ridges trends generally north to north–northwest and a secondary set trends generally east–west. Note how the plains surface generally decreases in elevation to the east across wrinkle ridges (red to yellow, yellow to green, green to blue, etc.), suggesting they accommodate elevation offsets via deep-seated faulting. Subtle arches between and adjacent to many ridges can also be seen that are likely structurally related to the wrinkle ridges, but could not be seen in visible images. Ridge rings, interpreted as wrinkle ridges that follow the rims of shallowly buried craters, can be seen at 10°N, 296°E and at 18°N, 296°E. MOLA data are from the 0.5 km gridded product (Smith *et al.*, 2001), illuminated from the south. The map is 720 km wide; each degree is about 60 km.

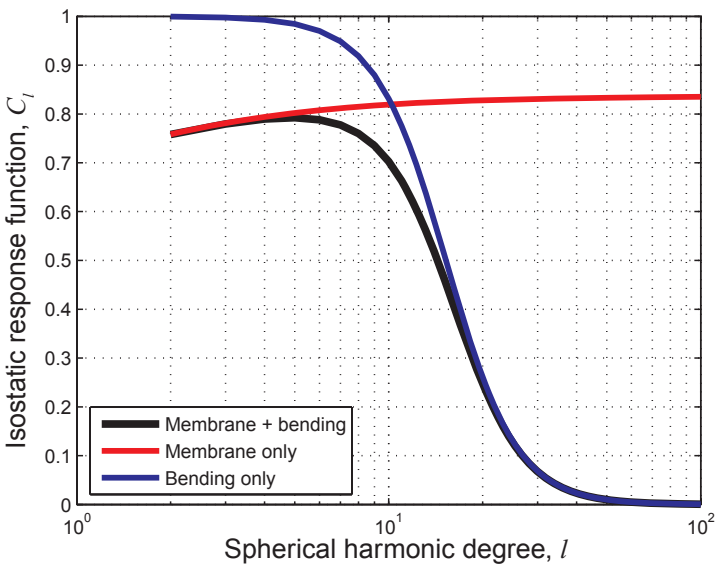

Plate 19. The "degree of compensation" or isostatic response function (Turcotte *et al.*, 1981), C_l, as a function of spherical harmonic degree, l, for a topographic load on a planetary lithosphere represented by a thin elastic spherical shell with a density contrast at its base. Perfect mass balance yields $C_l = 1$ and is possible at very long wavelengths (low spherical harmonic degree) when only bending forces are considered. The complete support of the load ("Membrane + Bending") is shown, as well as the responses obtained by isolating the membrane contribution and the bending contribution. For l less than about 10, the load is supported largely by membrane deformation. The elastic shell has a thickness, *Te*, of 100 km and a Young's modulus, *E*, of 5×10^{10} Pa. Crust and mantle densities are 2900 kg m^{-3} and 3500 kg m^{-3}, respectively.

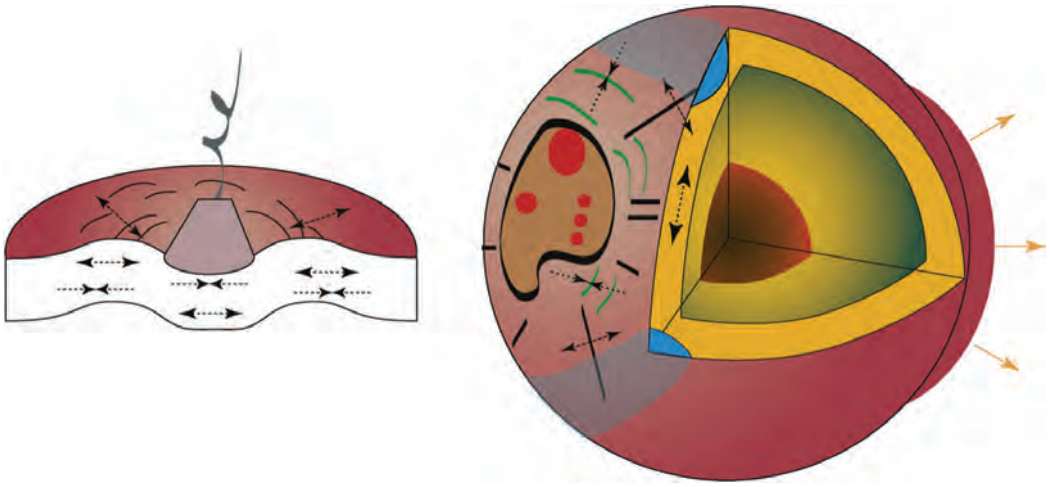

Plate 20. Stress modes on sphere and plate. Cartoon on left shows flexure on a flat elastic lithospheric plate with circumferential grabens resulting from radial extensional stresses in the flexural bulge surrounding the load. Cartoon on right indicates that for a large-scale load on a spherical elastic shell, the stress directions are switched relative to the flat plate due to the effects of membrane forces. A large load, relative to the radius of the planet, such as Tharsis, induces a trough or moat (gray) and an antipodal bulge (yellow arrows). This appears to explain the first-order gravity and topography of Mars. Outward black arrowheads indicate extensional stresses; inward black arrowheads indicate compressional stresses. Black lines and curves are graben; green curves are wrinkle ridges.

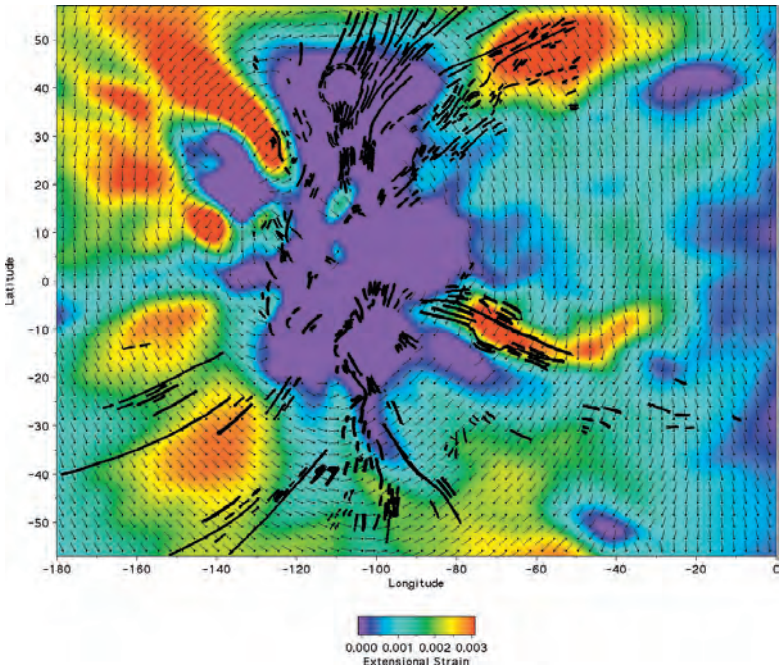

Plate 21. Extensional strain magnitude (color background) and direction (short lines) from model of elastic spherical shell loading as constrained by MGS gravity and topography data (Banerdt and Golombek, 2000). Major extensional structures are shown as heavier lines and are from Scott and Tanaka (1986). Results are shown for Tharsis (western) hemisphere. Model calculations use $T_e = 100$ km, crustal thickness = 50 km, crustal density = 2900 kg m^{-3} and mantle density = 3500 kg m^{-3}. Note structures are generally perpendicular to the extension direction, and the preponderance of structures in areas with high strain, such as Valles Marineris to the east–southeast, Tempe Terra to the northeast, Thaumasia to the south, and Sirenum to the southwest.

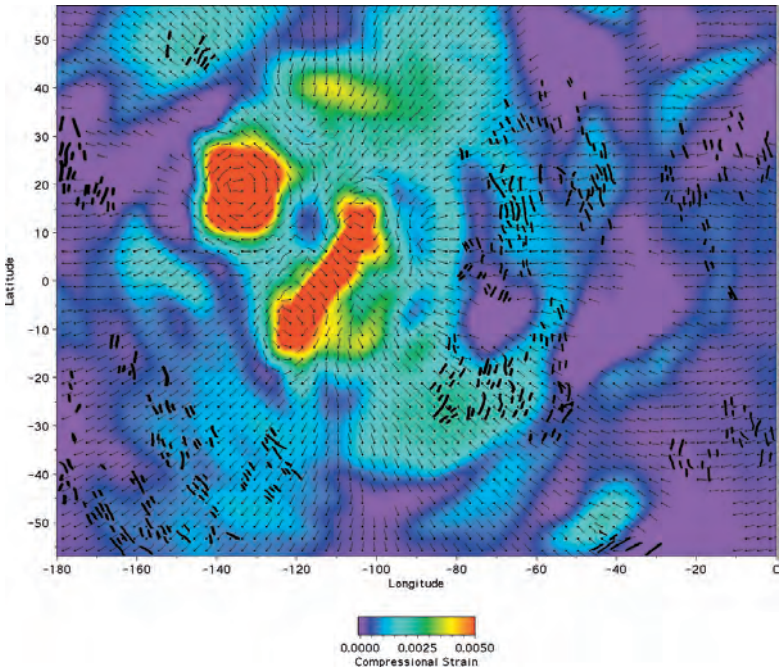

Plate 22. Compressional strain magnitude and direction from model (Banerdt and Golombek, 2000) described in Plate 21. Heavier lines are major wrinkle ridges from Scott and Tanaka (1986). Note structures are generally perpendicular to the compression direction, and the preponderance of structures in areas with relatively high strain, such as Lunae Planum to the east, Solis Planum to the southeast, Sirenum to the southwest, and Arcadia Planitia to the northwest.

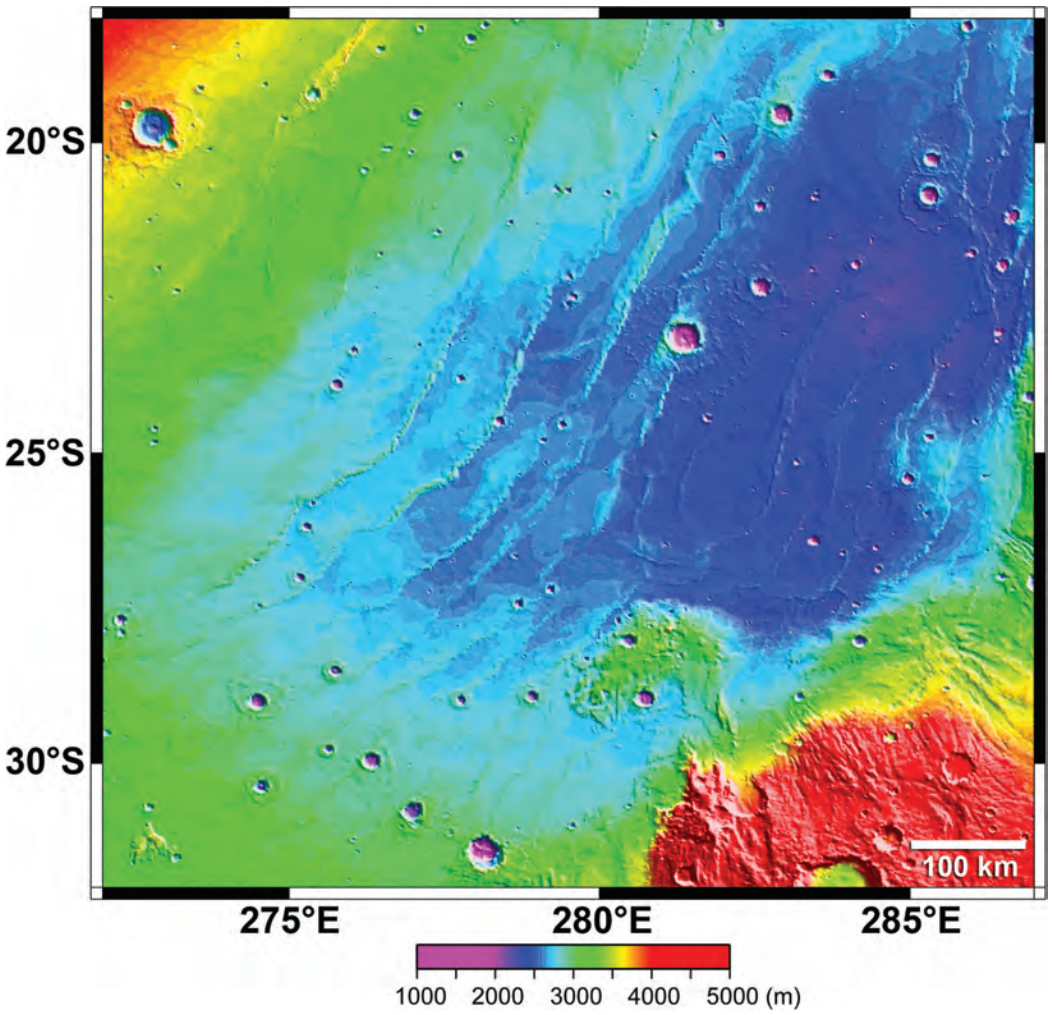

Plate 23. Ridged plains of Solis Planum, Mars. The color-coded shaded relief map generated using MOLA topographic data shows wrinkle ridges formed in ridged plains volcanic material partially filling a regional depression (see Watters, 2004). Narrow grabens and a possible rift cut highland areas at lower right. Topographic data are from the MOLA gridded 1/64° per pixel resolution model; artificial illumination from the left.

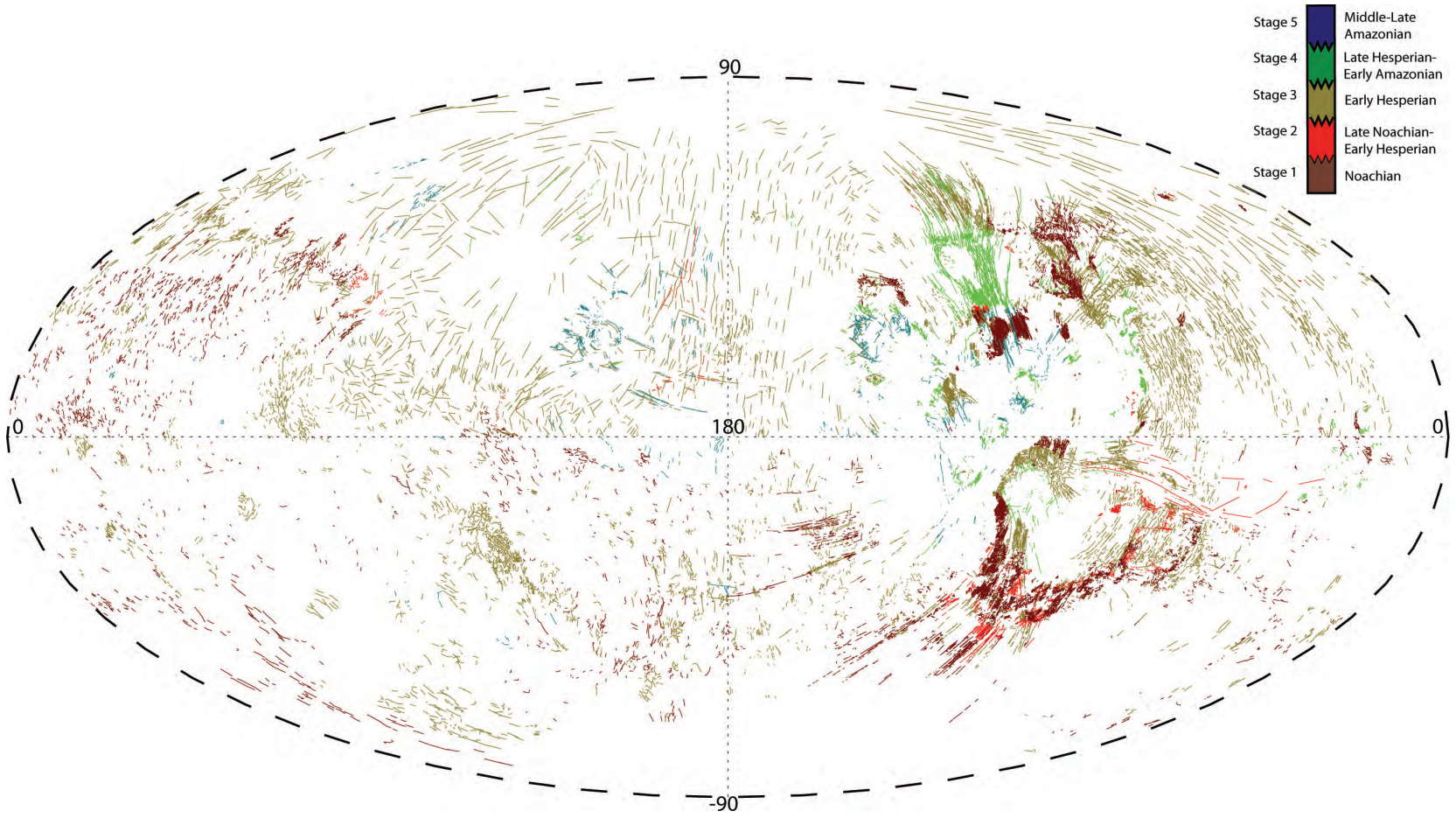

Plate 24. Map of tectonic structural features on Mars. Color coding reflects different ages of faults (grabens and wrinkle ridges) that relate to apparent major episodes of activity (adapted from Anderson *et al.*, 2001).

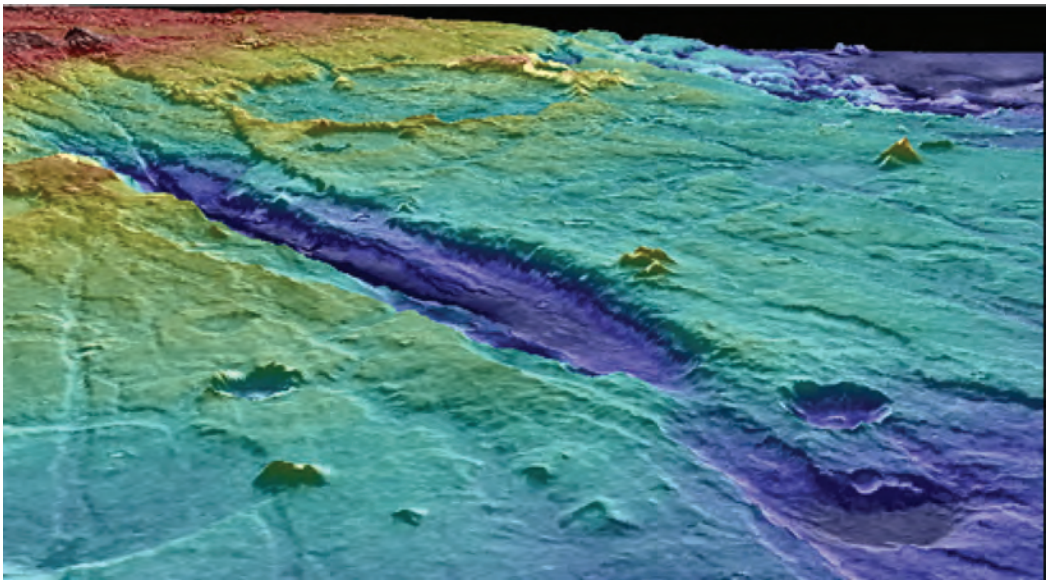

Plate 25. Oblique view of Tempe rift on Mars, looking southeast, created from MOLA DEM (Wilkins *et al.*, 2002; Okubo *et al.*, 2004). The main rift graben is ∼550 km long by ∼60 km wide and shows footwall uplift; many shallow grabens may represent an earlier stage of faulting in this part of northern Tharsis (e.g., Polit, 2005).